Materials Advances

ROYAL SOCIETY OF CHEMISTRY

PAPER

View Article Online
View Journal



Cite this: DOI: 10.1039/d6ma00145a

# Novel chitosan hybrid fluorinated thiourea derivatives as dual anti-microbial and anti-biofilm agents: tailoring molecular interactions, *in silico* toxicity, and docking simulation

Moustafa S. Abusaif, *[ab] Ahmed Ragab, *[bc] Mohamed A. Salem,[d] Nabila A. Maziad[e] and Yousry A. Ammar [b]

This article presents the synthesis of chitosan isothiocyanate, followed by hybridization with promising fluorinated aromatic amines, producing three chitosan fluorinated-thiourea samples (**CHTUD1–3**). Covalent modification of the chitosan and chitosan isothiocyanate backbones was confirmed by a notable reduction in ion exchange capacity (IEC). IEC decreased from 10.88 ± 0.23 for native chitosan and 3.21 ± 0.65 meq $g^{-1}$ for **CHNCS** to 4.25 ± 0.35 meq $g^{-1}$ for the final chitosan fluorinated-thiourea samples. This reduction strongly supports successful covalent grafting, meaning that the desired chemical modification was achieved. The modified chitosan (**CHTUD1–3**) was evaluated for antimicrobial activity. It showed significant effectiveness against the tested strains. These derivatives demonstrated significant antimicrobial activity, with MIC values ranging from 7.8 to 31.25 μg $mL^{-1}$ against Gram-positive strains, whereas native chitosan exhibited an MIC of 62.5 μg $mL^{-1}$. In contrast, the MIC values for Gram-negative strains ranged from 15.62 to 62.5 μg $mL^{-1}$, compared with native chitosan, which showed an MIC of 125 μg $mL^{-1}$ against the tested strains. The designed **CHTUD1–3** derivatives demonstrated significant antimicrobial activity against *S. aureus*, with an MIC of 7.8 μg $mL^{-1}$, which is significantly more promising than that of chitosan (62.5 μg $mL^{-1}$), indicating that chemical modification with fluorinated derivatives enhances antibacterial potency. Furthermore, these derivatives also showed potential against *C. albicans* with an MIC of 15.62 μg $mL^{-1}$, while native chitosan had an MIC of 62.5 μg $mL^{-1}$. Regarding biofilm inhibition, the percentages against *S. aureus* and *S. typhi* showed significant dose-dependent responses. Specifically, the new derivatives achieved ≥90% inhibition at 75% MBC and 70% inhibition at 25% MBC. However, **CHTUD2** exhibited 61.27% inhibition. *In silico* toxicity prediction revealed a favorable toxicity profile. Finally, molecular docking simulations revealed promising binding affinities. This suggests that these derivatives could inhibit biofilm formation by disrupting adhesion through sortase A and preventing biofilm formation *via* LpxC enzymes.

Received 31st January 2026,
Accepted 14th April 2026

DOI: 10.1039/d6ma00145a

rsc.li/materials-advances

## 1. Introduction

The emergence of multidrug-resistant organisms poses a serious global health concern, emphasizing the urgent need for new drugs capable of treating bacterial and fungal diseases.[1,2] So, creating and synthesizing new antimicrobial drugs remains a priority research goal. Out of them, novel promising aromatic compounds are being thoroughly examined as potential scaffolds to address microbial resistance to traditional treatments.[3,4] In the same vein, there is a substantial movement in the field of materials science toward the replacement of synthetic polymers with environmentally friendly materials that are generated from renewable sources.[5,6] Chitosan, defined as poly[(1 → 4)-β-linked 2-amino-2-deoxy-D-glucose], is a widely recognized natural polysaccharide,

[a] *Department for Synthesis and Characterization of Polymers, Polymer Institute of the Slovak Academy of Sciences, Dúbravská cesta 9, 845 41 Bratislava, Slovak Republic. E-mail: moustafa.samir@savba.sk*
[b] *Department of Chemistry, Faculty of Science (boys), Al-Azhar University, 11884 Nasr City, Cairo, Egypt. E-mail: mostafahozaifa317@azhar.edu.eg, ahmed_ragab@azhar.edu.eg*
[c] *Chemistry Department, Faculty of Science, Galala University, Galala City, Suez 43511, Egypt. E-mail: ahmed.abdelwahab@gu.edu.eg*
[d] *Health Specialties, Basic Sciences and Their Applications Unit, Applied College, Muhayl Asir, King Khalid University, Abha 62529, Saudi Arabia*
[e] *Polymer Chemistry Department, National Center for Radiation Research and Technology, Atomic Energy Authority, Cairo, Egypt*

typically sourced from the shells of crustaceans such as crabs, shrimp, and crawfish.[7,8]

Commercial production of chitosan, a notable semisynthetic polysaccharide, involves the partial deacetylation of chitin, the main structural component of crab shells. The result of this change is a polymer with new physicochemical properties, including increased bioactivity and enhanced solubility in acidic environments.[9] The resulting biomaterial is highly suitable for sophisticated applications due to its multitude of ''outstanding features.'' These features include biodegradability, biocompatibility, intrinsic antibacterial activity, and minimal immunogenicity. Chitosan (CH) also has moisturizing properties and is very hygroscopic.[10] Many industries, including medicine, food storage, farming, the textile industry, and environmental cleanup, utilize it because it possesses a strong set of qualities.[11,12] In addition, the expanding applications of chitosan necessitate the development of versatile derivatives through innovative modification technologies to meet current industrial and biomedical requirements.[13] The expanding applications of chitosan require the development of versatile derivatives through innovative modification technologies to meet current industrial and biomedical requirements.[14]

Chitosan's intrinsic activity, which stems from its abundance of hydroxyl and amino groups, makes it an ideal substrate for chemical modification. This flexibility is necessary for adjusting its physicochemical characteristics to particular applications.[15] Significant reaction pathways involve the nucleophilic amino groups, which readily react with some electrophiles like aldehydes or ketones to form Schiff base derivatives (–C═N–)[16,17] as well as acid chlorides or anhydrides to form amide derivatives (–CH–NH–CO–R),[18] and isothiocyanates to form thiourea derivatives (–CH–NH–CS–NH–R).[19] Among the distinguished functional derivatives of chitosan are the *N*-substituted thiourea compounds, which are generally synthesized through *N*-thiocarbamoylation utilizing isothiocyanate reagents. These analogs have shown great usefulness in a variety of applications. Some examples of thiourea chitosans include *N*-acetyl-, *N*-acyl-, *N*-fluoresceinyl-, and *N*-phenylthiourea chitosans.[20,21] One study found that an *N*-acetylchitosan thiourea derivative could be used as a corrosion inhibition material.[22] Another found that *N*-acyl-chitosans were effective antimicrobials,[23] and still another found that *N*-phenyl-chitosans were effective macromolecular fluorophores and metal adsorbents.[24,25] However, the commercial availability of the necessary isothiocyanate chemicals limits this synthesis process. A potentially more versatile strategy involves synthesizing a chitosan isothiocyanate intermediate. A polymer of this nature can subsequently undergo reactions with a diverse range of readily accessible amines, resulting in the formation of an extensive library of novel *N*-substituted thiourea derivatives. Notwithstanding this potential, and although the synthesis of glucosamine isothiocyanate derivatives *via* thiophosgene has been documented,[26] there is a conspicuous absence of reports concerning analogous chitosan isothiocyanate derivatives that employ the C-2 amino group. For more clarification, one document only reported the synthesis of acyl chitosan isothiocyanate derivatives and investigated their performance of photon-to-electron conversion, indicating that they may serve as a promising material for this application.[19]

Shibano and his colleagues developed a straightforward synthesis approach for acyl-chitosan isothiocyanates. This procedure employs a dual-phase approach: the initial *N*-phenylthiourea is achieved using phenyl isothiocyanate, followed by acylation through the application of either an acyl halide or an acyl anhydride. The intermediates produced consequently demonstrated improved solubility in the typically used organic solvents and were recognized as potentially useful precursors for the development of new functional chitosan derivatives.[27] Qin *et al.* reported the synthesis of three innovative thiosemicarbazone chitosan derivatives through a condensation reaction involving thiosemicarbazide chitosan and three different aromatic aldehydes: benzaldehyde, 2-hydroxybenzaldehyde, and 4-methoxybenzaldehyde. The *in vitro* antimicrobial and antifungal activity of these compounds was then tested against four prevalent crop-threatening pathogenic fungi and was found to be a remarkably effective material.

On the other hand, the strategic incorporation of specific functional groups serves as a fundamental approach to bestow novel properties upon a modified compound. The thiourea subunits, in particular, are well-known as beneficial components in various areas of study, including medicinal chemistry and organic synthesis.[28] Urea/thiourea compounds have gained popularity in recent years owing to their valuable chemical and biological characteristics. Both the acidity of the adjustable NH protons and their ability to function as hydrogen-bond donors make them among the most often used groups in the creation of organocatalysts and anion sensors.[29] Additionally, the capacity to form H-bonds has enabled the implementation of applications in crystal engineering and as membrane transporters.[30] The thiourea group serves as a crucial pharmacophore, characterized by its N–H groups and sulfur atom, which function as hydrogen bonding domains.[31] This structure is linked to a wide range of biological activities, encompassing anti-HIV,[32] analgesic,[33] antibacterial,[34] antitumor,[35] antifungal,[36] antiviral,[37] and anti-inflammatory properties,[38] among others. Moreover, the deliberate incorporation of fluorine or fluorine-containing groups, such as the trifluoromethyl ($-CF_3$) moiety, has become a significant strategy in the advancement of biologically active compounds.[39,40] The trifluoromethyl group in heterocyclic chemistry is notable for its capacity to modify the physicochemical and biological properties of the parent molecule.[41] The insertion of fluorine alters important steric and electronic characteristics, impacting a drug's pharmacological and pharmacokinetic effects. The trifluoromethyl group has a distinctive profile in terms of bioisosterism, as it is sterically larger than a methyl group and smaller than an isopropyl group.[42,43] The numerous US FDA-approved medications that contain fluorinated scaffolds are a testament to the potent pharmacological utility of these structures.[44]

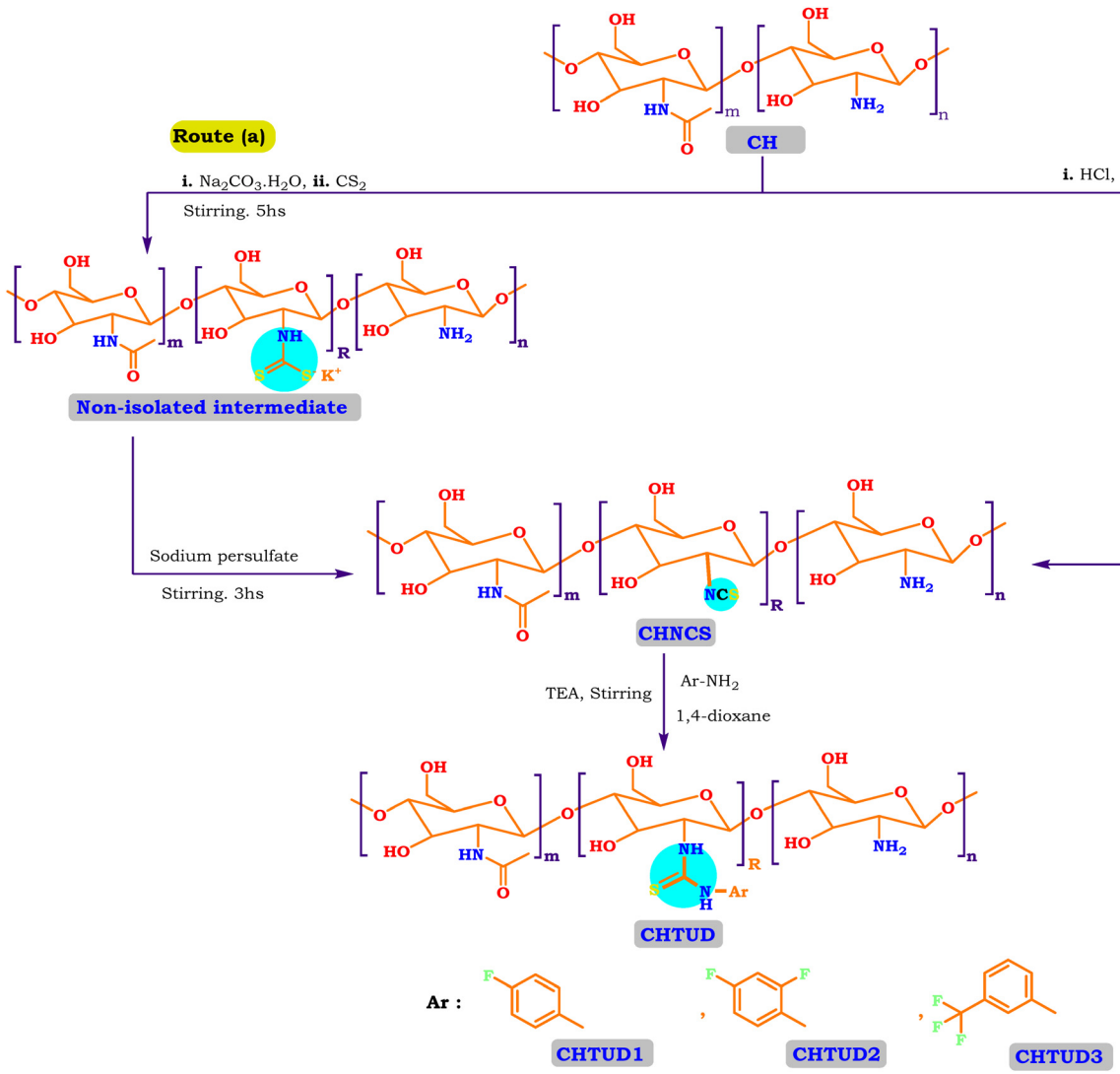


Scheme 1 Various synthetic pathways of novel chitosan isothiocyanate (**CHNCS**) and chitosan thiourea derivatives (**CHTUD**).

Among potential modifications, the combination of modified chitosan isothiocyanate with the aromatic fluorinated moiety is of particular interest. This approach utilizes the potential for a complementary or synergistic effect, given that both moieties exhibit recognized antimicrobial properties. There is a high probability that incorporating quinoxalines, known for their potent biological activity, will enhance the natural bioactivity of chitosan. This strategy aims to develop robust derivatives that demonstrate enhanced effectiveness for applications in biomedical and environmental fields.

So, the article describes in depth a novel approach to synthesizing modified chitosan isothiocyanates *via* two different pathways. This study also examines the reactivity of these isothiocyanates with promising fluorinated amines (Scheme 1). This significant modification, not previously documented, is expected to produce a material with notably improved antimicrobial properties, making it suitable for a range of medical and environmental uses. Finally, we assessed the efficacy of these samples as antimicrobial agents through *in vitro* assays targeting the pathogenic bacteria *B. subtilis* (ATCC 6633), *S. aureus* (ATCC 6538), *K. pneumoniae* (ATCC 13883), and *S. typhi* (ATCC 6539), as well as the fungus *C. albicans* (ATCC 10221).

## 2. Experimental section

### 2.1. Materials

Chitosan, a white powdered solid, was acquired from Qingdao Yunzhou Biochemistry Co., Ltd in China, exhibiting an 85% deacetylation degree and an average molecular weight of 40 KDa g $mol^{-1}$. *P*-Fluoroaniline (FA; purity = 98%, ID = 9349), 2,4-difluoroaniline (DFA; purity = 99%, ID = 9328), and *m*-trifluoromethyl aniline (TFA; purity = 96%, ID = 7097) were obtained from ChemSpider, United Kingdom. Carbon disulfide ($CS_2$; purity ≥95%, ID = 1131) was acquired from CAMEO Chemicals, United States, while sodium persulfate (SPS; purity ≥99%, ID = 71 889), thiophosgene ($CSCl_2$; purity ≥97%, ID = 79 380), and triethylamine ($Et_3N$; purity ≥99.5%, ID = 90 335)

were obtained from Sigma Aldrich, Germany. The required solvents, like 1,4-doxane ($Et_3N$; purity ≥99.8%, ID = 57 648 388) and acetone (C), were purchased from Sigma Aldrich, Germany. Ammonia solution ($NH_4OH$; 26%) was acquired from El-Nasr company, Egypt.

### 2.2. Assessments

**2.2.1. Substitution degree and ion exchange capacity.** The Kjeldahl method was utilized to ascertain the nitrogen content (*N*%) in both native chitosan and modified chitosan thiourea derivatives. The degree of substitution (DS) was subsequently calculated from these data using the following equation:[45]

$$\mathrm{DS} = 1 - \frac{M_b \times N_b}{M_a \times N_a} \quad (1)$$

where $M_b$ is the molecular weight of the glucosamine unit, and $M_a$ is the molecular weight of the substitution-modified chitosan, whereas $N_b$ denotes the nitrogen concentration in the untreated chitosan, $N_a$ refers to the nitrogen content in the chitosan thiourea derivatives.

We used a back-titration approach to find the ion exchange capacities (IECs) of the functionalized derivatives (**CHNCS**, **CHTUD1–3**) and native chitosan (**CH**). Samples with known weights were submerged in a 0.1 M $H_2SO_4$ solution for 10 hours. After filtration, the residual acid in the filtrate was measured through titration using a 0.1 N NaOH standard solution. A blank titration (without a sample) was conducted as a control. The IEC was then determined based on the data using the following equation:[46]

$$\mathrm{ICE}\left(\mathrm{meq\ g^{-1}}\right) = \frac{(V_2 - V_1)N}{W} \quad (2)$$

where $V_1$ represents the volume of NaOH consumed to neutralize the $H_2SO_4$ without the tested samples, and $V_2$ represents the volume of NaOH consumed to neutralize the $H_2SO_4$ with the tested samples. Additionally, *N* indicates the normality of the basic solution, while *W* signifies the weight of the investigated sample.

**2.2.2. Instrumental analytical methods.** We used a Shimadzu FTIR-8400 S (Kyoto, Japan) to capture the Fourier transform infrared spectra of the **CHNCS** and **CHTUD1–3** modified chitosan thiourea derivatives that we produced. A spectral range of 4000–400 $cm^{-1}$ was analyzed at 25 °C. The spectra were averages of sixteen scans, acquired using a 60 N universal compression force per cycle.

The proton signals of the three newly synthesized thiourea derivatives (**CHTUD1–3**) were meticulously characterized through the application of $^1H$ NMR spectroscopy. Spectra were obtained using a JEOL JNM-ECA 400 II spectrometer (Japan) functioning at a frequency of 400 MHz. Samples were solubilized utilizing trifluoroacetic acid (TFA-d) and DMSO-$d_6$ as the solvents of choice.

An X-ray diffraction (XRD) analysis was performed on the samples using Cu-Kα radiation on a PW1830 diffractometer (Japan). This allowed for the examination of the materials' crystalline structure.[47] We gathered data throughout a $2\theta$ scanning range that extended from 5° to 50°. To determine the crystalline index ($C_I$), the following equation was employed. This equation is based on the peak height measurements of the crystalline region (110) and the amorphous region ($I_{am}$).

$$C_I = \frac{I_{110} - I_{am}}{I_{110}} \times 100\% \quad (3)$$

In the above formula, $I_{110}$ indicates the highest intensity at $2\theta$°, and $I_{am}$ corresponds to the intensity of amorphous diffraction at 15.7°.

The thermal stability of native chitosan and the synthesized derivatives was assessed utilizing a TGA (SDT Q600 V20.9 Build 20). The samples were subjected to heating from ambient temperature to 600 °C at a constant rate of 10 °C $min^{-1}$ within a nitrogen atmosphere, with a flow rate of 5 mL $min^{-1}$ maintained. The integrated TA-50WSI thermal analysis system was utilized for data collection and management.

Moreover, the surface morphology of the native chitosan and the modified chitosan thiourea derivatives (**CHTUD1–3**) was examined utilizing a JEOL JSM-6360LA scanning electron microscope (SEM) from Tokyo, Japan. Micrographs were acquired using an accelerating voltage of 10.0 kV, with initial magnifications set at ×1000 and ×2000.

### 2.3. Synthetic methods

**2.3.1. Synthesis of modified chitosan isothiocyanate (CHNCS).** Route (a): chitosan isothiocyanate was synthesized through a one-pot method, wherein the synthesis of the non-isolable potassium dithiocarbamate chitosan intermediate followed the established protocol in the literature with slight modifications.[48] A suspended solution of chitosan (10 mmol, 1.6 gm) and potassium carbonate (20 mmol, 2.76 gm) was stirred in de-ionized water (20 mL) solution at room temperature for 1 h. After that, carbon disulfide (15 mmol, 0.904 mL) was added dropwise to the mixture over 30 min, and then the reaction mixture was stirred for 5 h to obtain the intermediate thiocarbamate derivative. Next, the pH of the mixture was adjusted to 7.4, the temperature was reduced to 0–2 °C, sodium persulfate (10 mmol, 2.38 gm) was added as an oxidizing agent portion-wise, and the solution mixture was stirred at r.t. for 3 h. After the reaction completion, the suspended mixture was filtered off using a Buchner funnel, washed several times with de-ionized water, and dried under vacuum. Chitosan isothiocyanate (**CHNCS**) is obtained as a pale-white powder, see Scheme 1.

Route (b): native chitosan (10 mmol, 1.6 gm) was dissolved in an aqueous hydrochloric acid solution with a pH of 2.5 while being stirred for 3 h at 0 °C to obtain a clear homogeneous solution. Then, thiophosgene (12 mmol, 0.912 mL) was added to the chitosan solution in one portion. Stirring immediately started at room temperature until the red color of thiophosgene completely disappeared, followed by a proper quantity of pure acetone being added to the mixture, resulting in the formation of the isocyanate derivative. The pale-white precipitate was filtered out, freeze-dried for 3 h, washed several times with acetone, and dried in a vacuum with $N_2$ bubbling. Also,

chitosan isothiocyanate (**CHNCS**) is obtained as a pale-white powder (Scheme 1).

**2.3.2. Synthesis of modified chitosan thiourea (CHTUD) derivatives.** To a suspended solution of chitosan isothiocyanate **CHNCS** (3 mmol, 0.480 gm) in 15 mL of anhydrous 1,4-dioxane containing TEA (1 mmol, 0.139 mL) as a basic catalyst, the appropriately selected fluorinated amines, such as *p*-fluoroaniline (3 mmol, 0.284 mL), 2,4-difluoroaniline (3 mmol, 0.307 mL), and *m*-trifluoromethyl aniline (3 mmol, 0.374 mL), were added and then the mixture was stirred at 50 °C for 14 h. After completion of the reaction, the pH of the solution mixture was adjusted to be neutral, and the solid precipitate was filtered out and washed several times with methanol, and dried at 60 °C to obtain *p*-fluorophenyl thiourea chitosan (**CHTUD1**), 2,4-difluorophenyl thiourea chitosan (**CHTUD2**), and *m*-trifluoromethylphenyl thiourea chitosan (**CHTUD3**) derivatives as presented in Scheme 1.

## 2.4. Antimicrobial evaluation

**2.4.1. Microbial strains.** The antimicrobial efficacy of the synthesized compounds was assessed against a selection of clinically significant microorganisms. This panel comprised the Gram-positive bacteria *Bacillus subtilis* and *Staphylococcus aureus*, the Gram-negative bacteria *Klebsiella pneumoniae* and *Salmonella typhi*, as well as the fungal strain *Candida albicans*. This selection facilitated a thorough evaluation of the compounds' antibacterial and antifungal capabilities.

**2.4.2. *In vitro* anti-microbial activity.** The assessment of anti-microbial activity was conducted utilizing the agar well diffusion method in accordance with CLSI guidelines. In this approach, the agar surface was inoculated with a microbial suspension, and wells (6–8 mm in diameter) were aseptically prepared and filled with 100 μL of the test solutions at the desired concentrations. The chitosan and modified chitosan were used at a concentration of 50 mg $mL^{-1}$. In comparison, the positive control drugs (ampicillin and nystatin) were used at 10 mg $mL^{-1}$, where these samples were dissolved at their concentration in 1 mL of DMSO (5%). To assess antimicrobial potency, inhibition zones were measured in millimeters after incubation under appropriate conditions (16–24 hours for bacteria and up to 48 hours for fungi) as described previously.[49] This method allows for both qualitative and quantitative evaluation of compounds' antimicrobial properties.

**2.4.3. MIC and MBC/MFC determination.** In this study, the minimum inhibitory concentration (MIC) was established as the concentration at which observable microbial growth is entirely suppressed and assessed as previously outlined, with several modifications.[50] We calculated the MICs of the substances examined using a conventional broth dilution approach. To prepare 1000 μg $mL^{-1}$ stock solutions, 10 mg of each sample was dissolved in 10 mL of deionized $H_2O$. Serial two-fold dilutions were then performed to achieve a concentration range of 1000 to 3.25 μg $mL^{-1}$. Each dilution was incubated under appropriate conditions after being inoculated with a standardized microbial suspension. Subculturing 0.1 mL from wells or tubes that did not exhibit apparent growth in the MIC test onto new Sabouraud dextrose agar plates allowed us to calculate the minimum bactericidal concentration (MBC) or minimum fungicidal concentration (MFC). The lowest concentration that exhibited no colony formation during incubation was recorded as the MBC for bacteria or MFC for fungi, indicating that viable microbial cells had been eliminated.

**2.4.4. Biofilm activity.** Microplate assays were conducted to assess the anti-biofilm activity of the tested derivatives **CHTUD1–3** using the crystal violet (CV) microtiter plate assay.[51] In each well of the 96-well flat-bottom microplate, we added 300 μL of freshly inoculated tryptic soy yeast broth containing approximately $10^6$ CFU per mL of the test organism. We tested the concentrations of each compound at 75%, 50%, and 25% of the MBC values, while the controls contained only the medium or solvent. After incubation at 37 °C for 48 hours, the plates were rinsed with sterile distilled water to eliminate non-adherent cells. The residual adherent biofilms were subsequently stained with a 0.1% crystal violet solution for 15 minutes. Following rinsing and air-drying, the bound dye was solubilized in 95% ethanol, and absorbance was measured at 570 nm using a microplate reader. The calculation of biofilm inhibition percentage was performed using the following formula:

$$\text{Biofilm inhibition (\%)} = [1 - (A_{\text{control}} - A_{\text{blank}})(A_{\text{sample}} - A_{\text{blank}})] \times 100$$

**2.4.5. Molecular docking simulation.** To elucidate the binding mode and propose a potential mechanism of action, as well as to visualize the binding interactions of the modified thiourea chitosan derivatives **CHTUD1–3**, molecular docking simulations were performed targeting the active sites of sortase A (PDB: 1T2P) (https://www.rcsb.org/structure/1T2P; last accessed on 22/10/2025) and LpxC (PDB: 4IS9) (https://www.rcsb.org/structure/4IS9; last accessed on 22/10/2025). The docking process was performed using Molecular Operating Environment Software version 10.2009.[52–54] First, the structure of the modified chitosan derivatives was generated and exported to MOE, as described previously.[55] To create the active site of sortase A (PDB: 1T2P), we employed the dummy atoms method under default conditions for chain A, specifying 137 amino acid residues to obtain the active site. Next, we isolated the active site of the pocket using a standard protocol. For LpxC (PDB: 4IS9), the validation process revealed that the co-crystallized ligand exhibited a binding affinity of −8.67 kcal $mol^{-1}$, with an RMSD value of 0.965, as presented in Fig. S7–S9. This validation process was conducted using only chain A along with the protonated 3D structure, minimized energy, and isolated active sites. The redocking process showed that the co-crystallized ligand maintained an RMSD value of 0.965 throughout the formation, with one hydrogen bond formed between the oxygen of the carbonyl related to the oxazole nucleus, featuring a bond length of 1.8 Å and a strength of 33% (Fig. S7–S9). SI contains all docking figures for validation and the full size of each docking figure, represented as Fig. S1–S15.

# 3. Results and discussion

## 3.1. Synthesis of the chitosan thiourea (CHTUD) derivative

Nucleophilic addition reaction involving isothiocyanate and variable amines represented a widely accepted approach for the synthesis of thiourea derivatives.[56,57] But, due to the high cost and unavailability of all required isothiocyanate derivatives to react with chitosan, the authors planned to construct a modified chitosan isothiocyanate to be available to react with variable amines. Also, in the synthetic methodologies pertaining to chitosan thiourea (**CHTUD1–3**), novel chitosan isothiocyanate (**CHNCS**) emerged as a significant intermediate. In this study, the **CHNCS** key intermediate can be achieved through two routes: (a) through elimination reaction of non-isolable chitosan carbamodithioate using sodium persulfate; (b) through a one-step reaction of chitosan with thiophosgene in an acidic medium. For more details on route (a), chitosan isothiocyanate (**CHNCS**) was produced in a one-pot synthesis by combining chitosan with carbon disulfide in a basic medium, which afforded the non-isolable chitosan carbamodithioate, then subsequently eliminated using sodium persulfate (Scheme 1). This approach prevented the isolation and purification of each synthesized intermediate, thereby conserving time, solvents, and energy-intensive processes. Also, this approach is explained using the suggested mechanism as depicted in Fig. 1 under ideal circumstances. In a basic environment, an amine attacks the electrophilic carbon of carbon disulfide ($CS_2$) to generate a carbamodithioic acid. This acid, when combined with a base, forms a stable dithiocarbamate salt. The amine attacks the central carbon of $CS_2$, generating a zwitterionic intermediate (route a). The base subsequently deprotonates it to create the dithiocarbamate salt, a flexible intermediate for future reactions. Next, the following step involved the conversion of non-isolable dithiocarbamate salt to the corresponding isothiocyanate compound (**CHNCS**).[58] It is widely recognized that the persulfate anion

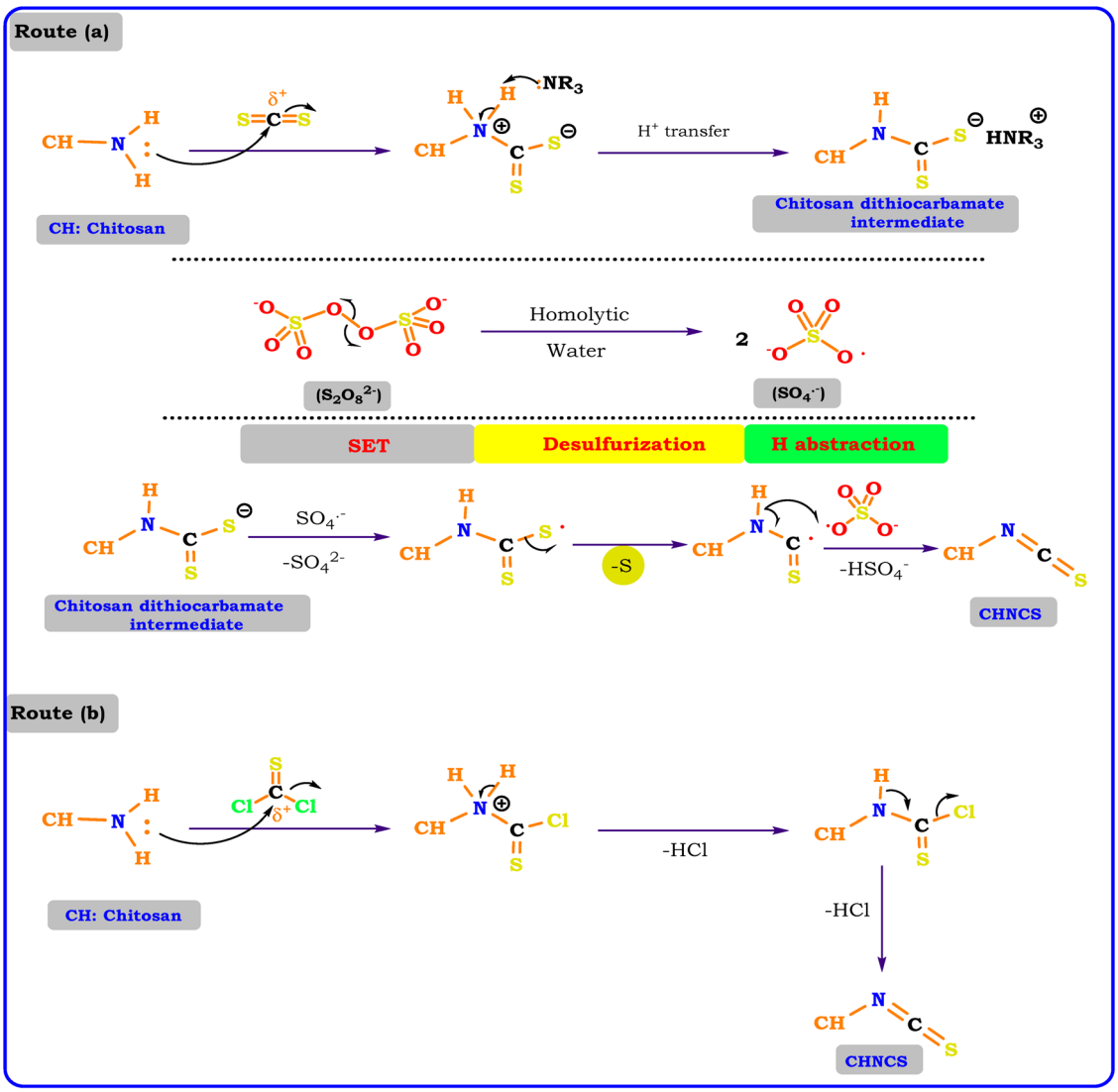


Fig. 1 The mechanism illustrates the two different routes of preparation of chitosan isothiocyanate (**CHNCS**).

Table 1 Elemental analysis found and calculated, and degree of substitution (DS) of the synthesized CH–isothiocyanate and CH–thiourea derivatives

| Sample | Yield[a] (%) | Color | Elemental analysis, calcd (found)[b] (%) | | | | DS[c] | DS[d] |
|---|---|---|---|---|---|---|---|---|
| | | | C | N | H | C/N | | |
| **CH** | — | White | 45.22 (46.02) | 8.10 (7.67) | 7.27 (6.90) | 45.22 (46.02) | — | — |
| **CHNCS** | 66.7 | Pale white | 44.70 (44.36) | 7.98 (7.39) | 6.53 (6.03) | 44.70 (44.36) | 0.54 | — |
| **CHTUD1** | 73.4 | Light yellow | 46.23 (47.51) | 8.89 (8.24) | 6.44 (6.93) | 46.23 (47.51) | 0.51 | 0.47 |
| **CHTUD2** | 78.5 | Yellow | 45.87 (46.48) | 8.77 (8.03) | 6.07 (5.63) | 45.87 (46.48) | 0.52 | 0.45 |
| **CHTUD3** | 84.3 | Orange | 45.21 (46.77) | 8.90 (7.52) | 4.87 (5.82) | 45.21 (46.77) | 0.50 | 0.46 |

[a] Yield is the ratio of CH–isothiocyanate and CH–thiourea derivative. [b] Theoretical elemental analysis based on the empirical formula of $(C_8H_{13}NO_5)_m(C_6H_{11}NO_4)_n(C_6H_{10}NO_4$ + thiourea moiety$)_{n-z}$, where $m$ = 0.15 (molar ratio of chitin), $y$ = 0.85 is the degree of deacetylation of CH and $z$ is the experimental value of the DS of the prepared CH–thiourea derivative. [c] Degree of substitution of the CH–isothiocyanate and CH–thiourea derivative determined from elemental analysis. [d] Degree of substitution of the CH–thiourea derivatives determined from $^1$H NMR.

readily experiences homolytic cleavage in solutions, resulting in the formation of a sulfate radical anion. Single electron transfer (SET) from the chitosan dithiocarbamate intermediate to the sulfate radical anion generates carbamodithionyl radicals (**A**) and releases the sulfate anion. The process of desulfurization of carbamodithionyl radicals (**A**) continues, leading to the formation of carbamothionyl radicals (**B**), which the radical scavenger TEMPO may intercept. The sulfate radical anion abstracts hydrogen from carbamothionyl radicals (**B**), resulting in the formation of isothiocyanates (**CHNCS**) see Fig. 1.

Moreover, chitosan isothiocyanate (**CHNCS**) is produced using another synthetic pathway through one step, which involves the reaction of chitosan with thiophosgene in an acidic medium, and the suggested mechanism is depicted in Fig. 1 (route b). The interaction between an amine function in the chitosan skeleton and thiophosgene ($CSCl_2$), leading to the formation of an isothiocyanate (CH–N═C═S), occurs through a nucleophilic attack by the amine on the electrophilic carbon of thiophosgene. This process results in the generation of an intermediate, followed by the elimination of two molecules of hydrogen chloride (HCl). Firstly, the nucleophilic nitrogen atom of the principal amine hits the electrophilic carbon atom in the middle of thiophosgene ($CSCl_2$).[59] In doing so, it splits the double bond between carbon and sulfur and creates a tetrahedral intermediate. A proton is transferred from nitrogen to one of the chlorine atoms, and concurrently or in a subsequent step, one molecule of HCl is eliminated, resulting in the formation of a thiocarbamoyl chloride intermediate. The removal of the second molecule of HCl results in the synthesis of the desired isothiocyanate (**CHNCS**) along with a base molecule or residue.

Finally, the chitosan isothiocyanate structure (**CHNCS**) is used as an electrophile through its reaction with some promising selective amines, fluoroaniline, difluoroaniline and trifluoromethylaniline, which furnished the target thiourea derivatives, **CHTUD1–3**, respectively (Scheme 1). Amines undergo a reaction with isothiocyanates to yield thioureas, facilitated by the nucleophilic attack of the amine on the electrophilic carbon present in the isothiocyanate group. With the help of an alkaline setting and deprotonated amines, this reaction may generate a stable thiourea bond without the need for a leaving group.[60]

### 3.2. Calculations of substitution degree and ion exchange capacity assessments

Color and yield percentage of the chitosan isothiocyanate (**CHNCS**) and chitosan thiourea derivative (**CHTUD**) are assessed and depicted in Table 1. It was found that all product samples are different in color, which is more evidence for successful reactions. The **CHNCS** sample is obtained as a pale white color with 66.7% yield, while the corresponding thiourea derivatives (**CHTUD1–3**) are obtained as light yellow, yellow, and orange colors, with 73.4%, 78.5%, and 84.3% yield, respectively.

Furthermore, an elemental analysis was conducted to ascertain the substitution degree (DS) of the modified chitosan samples using eqn (4).[61]

$$\mathrm{DS} = \frac{a\left(\frac{C}{N}\right)m - \left(\frac{C}{N}\right)o}{n} \quad (4)$$

So, the degree of substitution of the **CHNCS** sample was 0.54, while the modified samples **CHTUD1–3** were found to be 0.51, 0.52, and 0.50, respectively. The presented results indicate that the DS of all modified chitosan samples is around 0.50. In certain instances, the antimicrobial efficacy may be influenced directly by the extent of substitution, as the thiourea function provides a platform for improving the bioactivity of chitosan thiourea derivatives. Elemental analysis was used to calculate the M.wt. of the formula $(C_8H_{13}NO_5)_{0.15}(C_6H_{11}NO_4)_{0.85}(C_6H_{10}NO_4$ + thiourea moiety$)_{0.85-z}$, and the determined DS ($z$) aligned with the DS that really occurred.

At the same time, assessments of ion exchange capacity (IEC) may reveal the preparation of new thiourea functionalities through the presence of the amine group ($NH_2$) within the chitosan framework. So, the IEC findings for the original chitosan indicated the highest value of 10.88 ± 0.23 meq g$^{-1}$. Chemical modification of chitosan into **CHNCS** resulted in a decrease in the IEC value of 3.21 ± 0.65 meq g$^{-1}$. Also, the three modified thiourea samples (**CHTUD1–3**) resulted in a reduction of the IEC value of 3.21 ± 0.65 meq g$^{-1}$. The IEC findings indicated reduced values of 3.89 ± 0.26, 4.25 ± 0.13, and 4.13 ± 0.35 meq g$^{-1}$, respectively. Moreover, the noted decrease can be ascribed to the chemical modification of chitosan into isothiocyanate or thiourea derivatives. In addition, the nitrogen atoms

Table 2 Solubility test of chitosan derivatives **CHNCS** and **CHTUD1–3** in various solvents

| | Solubility | | | | | | | |
|---|---|---|---|---|---|---|---|---|
| Sample code | Distilled $H_2O$ | 1% AcOH | DMSO | DMF | $CHCl_3$ | MeOH | EtOH | THF |
| **CH** | − | + | ± | − | − | − | − | − |
| **CHNCS** | − | − | ± | ± | − | − | − | − |
| **CHTUD1** | − | − | + | ± | ± | − | − | − |
| **CHTUD2** | − | − | + | ± | ± | − | − | − |
| **CHTUD3** | − | − | + | ± | ± | − | − | − |

Solubility parameter; + soluble; − insoluble; ± swell.

in the thiourea function (NH–CS–NH) did not affect the ion exchange capacity since they are not ionizable under the conditions tested. Consequently, under the experimental circumstances (employing 0.1 M $H_2SO_4$), the NH of thiourea function stays unprotonated and does not significantly affect the ion exchange capacity, owing to its acidic NH rather than fundamental nature. The changes observed in IEC can be primarily attributed to the development of the target function, rather than the protonation of the nitrogen. The measurements of ion exchange capacity (IEC) demonstrated a significant correlation with the observed degree of substitution.

### 3.3. Solubility test

The solubility characteristics of native chitosan (**CH**) and its modified derivatives (**CHNCS**, **CHTUD1–3**) were examined across a range of solvents, with the findings provided in Table 2. Native chitosan exhibited a distinct solubility profile: it was insoluble in distilled water due to extensive inter- and intramolecular hydrogen bonding, yet it dissolved readily in 1% acetic acid after the protonation of its amino groups. Chitosan demonstrated swelling in strong polar organic solvents such as DMSO, rather than achieving complete dissolution.[62] Chemical changes, on the other hand, drastically changed these characteristics. There was a significant decrease in the solubility of the **CHNCS** intermediate and the **CHTUD1–3** final thiourea derivatives in 1% acetic acid. The observed decrease in acid solubility indicates a substantial level of substitution, leading to a reduction in the availability of free amino groups for protonation. The derivatives demonstrated enhanced affinity for organic solvents; the modified thiourea samples (**CHTUD1–3**) exhibited high solubility in DMSO and displayed swelling behavior in DMF and $CHCl_3$. While the **CHNCS** intermediate was insoluble in most organic solvents, it was observed to swell in DMSO and DMF.

The inability of chitosan thiourea derivatives to dissolve in water and most organic solvents, along with their swelling capacity in polar solvents like DMSO and DMF, highlights their potential application in water purification systems. Insoluble materials serve as efficient adsorbents for pollutants, heavy metals, and pigments, as they can be readily recovered and reused without disintegrating in the treatment solution. The observed swelling behavior in polar solvents such as DMSO and DMF indicates a potential for matrix-controlled release of active agents. This may be utilized in applications including the creation of antimicrobial coatings or targeted remediation systems. Lastly, a shift in the solubility character is significant evidence for the successful synthesis of the modified thiourea samples (**CHTUD1–3**).

### 3.4. Instrumental characterization

**3.4.1. FT-IR spectrum.** The structural modification of the chitosan backbone has been determined through FTIR spectroscopy. The spectra of native chitosan (**CH**) and the chitosan isothiocyanate intermediate (**CHNCS**) are displayed in Fig. 2, with the principal absorption bands summarized in Table 3. The spectrum of native chitosan (Fig. 2a) exhibited the distinctive absorption bands associated with the polysaccharide. A prominent and robust band was detected in the 3450–3390 $cm^{-1}$ range, indicative of the overlapping stretching vibrations associated with O–H and N–H groups. Asymmetric C–H stretching vibrations were present at 2948 $cm^{-1}$ and 2860 $cm^{-1}$. The spectrum also showed two critical peaks in the amide region: a band at 1650 $cm^{-1}$ (C═O axial stretching of the residual acetamide group) and a peak at 1590 $cm^{-1}$ representing the N–H bending vibration of the primary amino group.[63] Asymmetric stretching of the C–O–C ether linkages and skeletal vibrations of the saccharide ring were attributed to the firm peaks at 1130 $cm^{-1}$, 1080 $cm^{-1}$, and 1020 $cm^{-1}$, respectively, in the fingerprint area, while absorptions at 1410 $cm^{-1}$ and 1390 $cm^{-1}$ were associated with $CH_3$ and $CH_2$ bending.[55] In contrast, the spectrum of the **CHNCS** sample (Fig. 2b) showed obvious indications of effective functionalization. The most prominent new feature was the appearance of a sharp, intense absorption band at 2071 $cm^{-1}$, characteristic of the asymmetric stretching vibration of the isothiocyanate (–N═C═S) functional group. Concurrently, there was a significant decrease in the intensity of the peak at around 1590 $cm^{-1}$, which was earlier designated as 1580 $cm^{-1}$ in the derivative and was related to the N–H bending of the primary amine. This weakening demonstrates that the substitution reaction devoured the principal amino groups.[19] Moreover, the residual acetamide signal exhibited a shift to 1628 $cm^{-1}$. The observed spectral alterations collectively validate the successful synthesis of the chitosan isothiocyanate (**CHNCS**) intermediate.

After modifying chitosan isothiocyanate to thiourea derivatives (**CHTUD1–3**), FT-IR charts of the thiourea derivatives indicate the lack of the characteristic band associated with the isothiocyanate group (–NCS) at 2070 $cm^{-1}$. The appearance of several new, significant peaks characterized the spectrum of **CHTUD1** (Fig. 2c). A strong band emerged at 1512 $cm^{-1}$, which

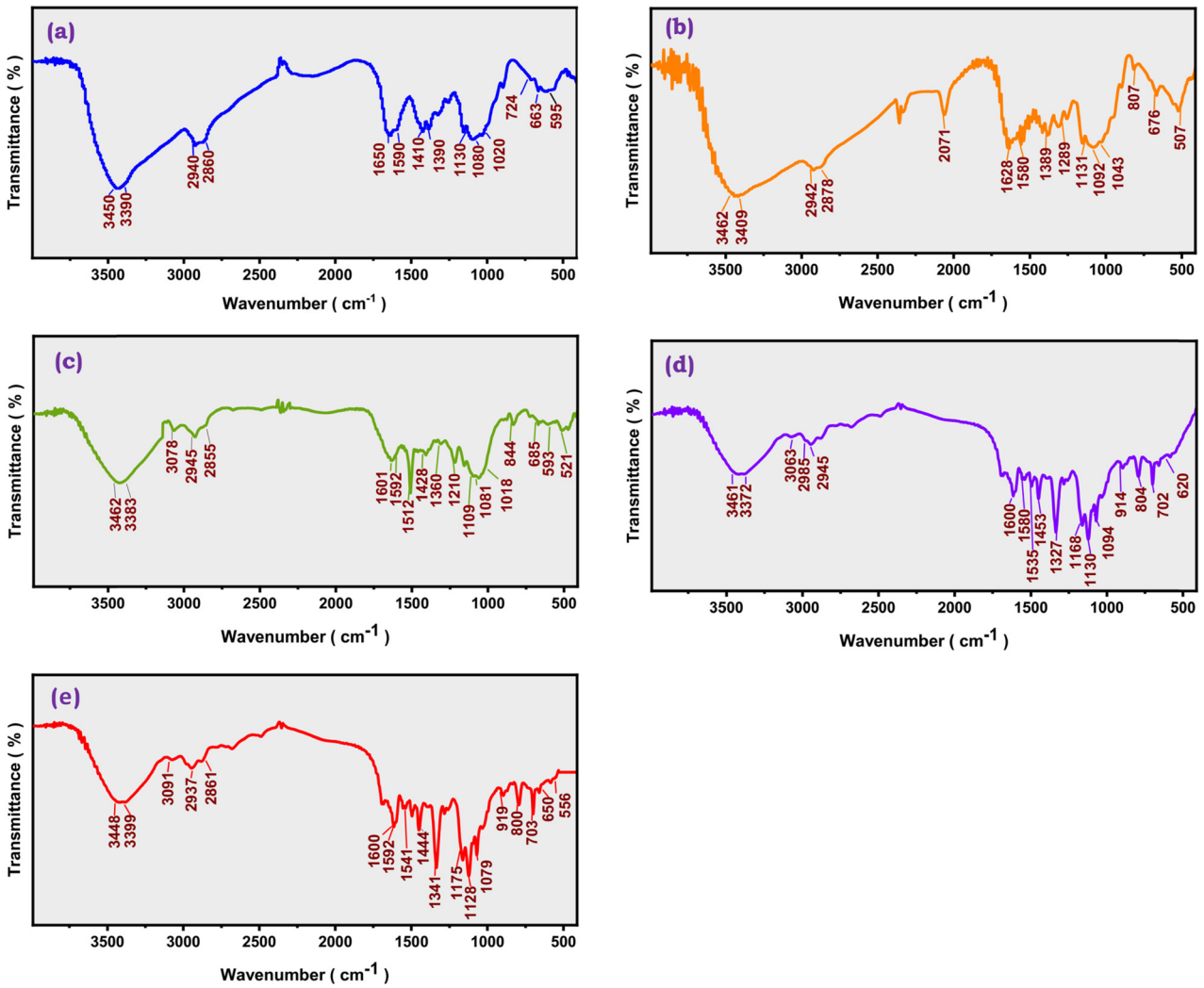


Fig. 2 FT-IR analysis of chitosan (a) and its modified isothiocyanate **CHNCS** (b) and thiourea derivatives **CHTUD1–3** (c–e).

is ascribed to the N–H bending and C═S stretching vibrations of the newly formed thiourea group (–NH–CS–NH–). Concurrently, additional bands at 3080 $cm^{-1}$ (aromatic $sp^2$ C–H stretching) and 1210 $cm^{-1}$ (C–F bond stretching) emerged, which validated the presence of the fluorinated phenyl moiety (Fig. 2c). Similar evidence was observed for **CHTUD2** (Fig. 2d). Its successful synthesis was indicated by the emergence of characteristic new bands at 1535 $cm^{-1}$ (–NH–CS–NH– group), 3063 $cm^{-1}$ (aromatic $sp^2$ C–H), 1327 $cm^{-1}$ (C–F stretching), and 702 $cm^{-1}$ (phenyl ring vibration). In the case of **CHTUD3** (Fig. 2e), unique absorption bands that corroborate the structure were detected at 1444 $cm^{-1}$ (associated with the

Table 3 Significant peak assignments and functions in the FT IR chart for the synthesized materials

| | FT IR ($\nu$/$cm^{-1}$) | | | | |
|---|---|---|---|---|---|
| | **CH** | **CHNCS** | **CHTUD1** | **CHTUD2** | **CHTUD3** |
| Compound | $-NH_2$ | –NCS | $-CS(NH)_2$–4-F–$C_6H_4$ | $-CS(NH)_2$–2,4-$(F)_2$–$C_6H_3$ | $-CS(NH)_2$–3-$CF_3$–$C_6H_4$ |
| OH and $NH_2$ stretching | 3450, 3390 | 3463, 3409 | 3462, 3383 | 3461, 3372 | 3448, 3399 |
| CH stretching ($SP^2$–CH) | — | — | 3078 | 3063 | 3091 |
| CH stretching ($SP^3$–CH) | 2940, 2860 | 2942, 2878 | 2945, 2855 | 2985, 2845 | 2937, 2861 |
| –NCS stretching | — | 2071 | — | — | — |
| C═O stretching ($NHCOCH_3$) | 1650 | 1628 | 1601 | 1600 | 1600 |
| $NH_2$ bending | 1590 | 1580 | 1592 | 1580 | 1592 |
| NH–CS–NH stretching | — | — | 1512 | 1535 | 1444 |
| –C–F stretching | — | — | 1210 | 1327 | 1341 |
| C–O–C stretching (glucoside linkage) | 1131, 1092 | 1131, 1092 | 1109, 1081 | 1130, 1094 | 1128, 1079 |

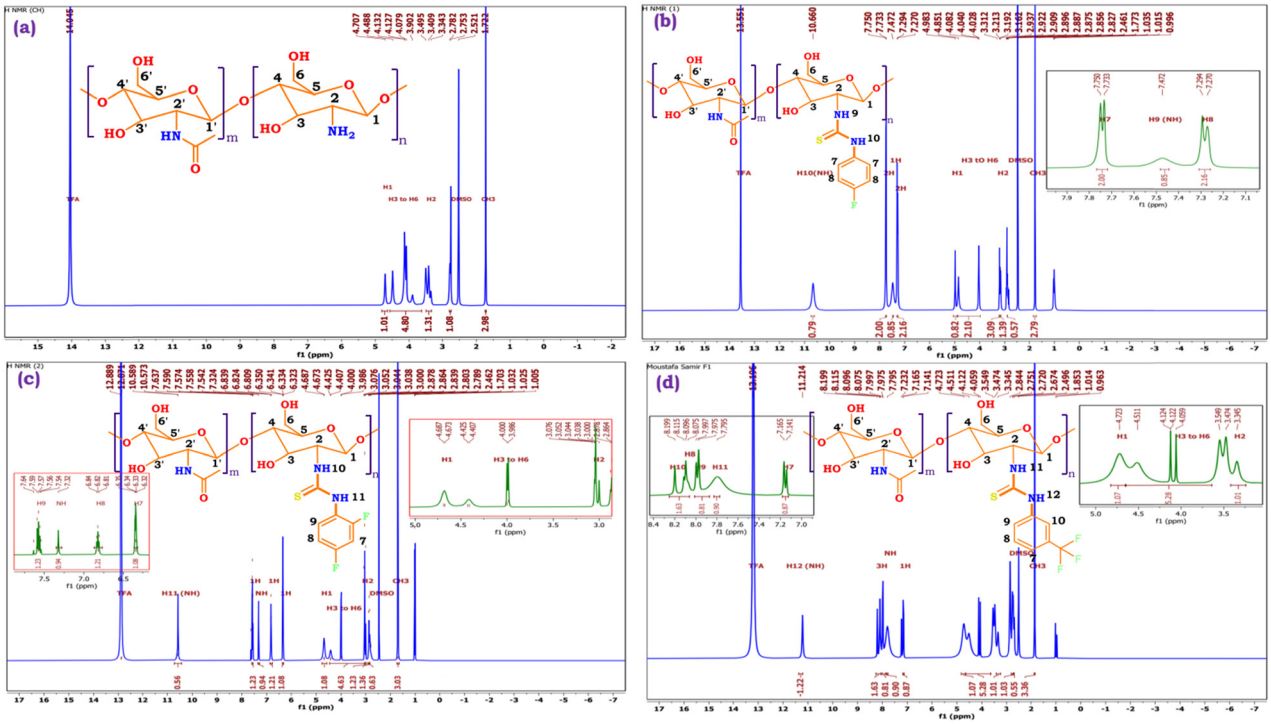


Fig. 3 $^{1}$H NMR analysis of chitosan (a) and its chitosan-modified thiourea derivatives **CHTUD1–3** (b–d).

–NH–CS–NH– linkage), 3091 cm$^{-1}$ (aromatic sp$^{2}$ C–H), 1341 cm$^{-1}$ (C–$F_3$ group), and 703 cm$^{-1}$ (phenyl ring). The primary absorption frequencies of the chitosan backbone, such as the wide O–H/N–H stretching (~3462–3383 cm$^{-1}$), the C–H stretching (~2945–2855 cm$^{-1}$), and the C–O–C skeletal vibrations (~1109–1018 cm$^{-1}$), were still present in all three of the derivative spectra (**CHTUD1–3**). This proves that the change did not damage the polysaccharide backbone.

The complete absence of the sharp–NCS peak (at 2071 cm$^{-1}$) alongside the emergence of new bands associated with the –NH–CS–NH– linkage and the distinct aromatic substituents serve as clear evidence that the phenyl thiourea derivatives have been effectively integrated into the chitosan backbone.

**3.4.2. $^{1}$H NMR spectrum.** $^{1}$H NMR spectroscopy is a crucial technique that is used to verify the successful modification and synthesis of chitosan-thiourea derivatives (**CHTUD1–3**). As displayed in Fig. 3 and Table 4, the $^{1}$H NMR chart of the native chitosan (**CH**) is depicted for comparison with the modified chitosan samples. The spectrum, obtained in a DMSO-$d_6$/TFA solvent solution, exhibits all the typical resonance signals anticipated for the chitosan polymer. The *N*-acetyl-D-glucosamine units include three methyl protons ($CH_3$) from the *N*-acetyl groups ($COCH_3$), which are responsible for the most prominent upfield signal, a singlet at $\delta$ 1.72 ppm. Around $\delta$ 2.52 ppm, the solvent peak for DMSO-$d_6$ has appeared. Near the protonated amine group, at $\delta$ 2.75 ppm and $\delta$ 2.78 ppm, are the signals for the $H_2$ proton of the D-glucosamine (deacetylated) units (Fig. 3a). Between $\delta$ 3.41 ppm and $\delta$ 4.49 ppm, a complicated area of multiplets is observed that corresponds to the non-anomeric protons of the glucopyranose ring ($H_3$–$H_6$). The $\delta$ 4.71 ppm signal unambiguously identifies the anomeric proton ($H_1$) of the polysaccharide backbone.[64] The strong

Table 4 $^{1}$H NMR assignments of chitosan and modified chitosan thiourea derivatives

| | $^{1}$H NMR ($\delta$/ppm) | | | |
|---|---|---|---|---|
| | **CH** | **CHTUD1** | **CHTUD2** | **CHTUD3** |
| Compound | –$NH_2$ | –$CS(NH)_2$–4-F-$C_6H_4$ | –$CS(NH)_2$–2,4-$(F)_2$–$C_6H_3$ | –$CS(NH)_2$–3-$CF_3$–$C_6H_4$ |
| $CH_3$ ($NHCOCH_3$) | 1.72 | 1.77 | 1.80 | 1.85 |
| $H_2$ | 3.40 | 3.16 | 3.01 | 3.34 |
| $H_3$, $H_4$, $H_5$, $H_6$ (non-anomeric) | 3.49–4.48 | 3.31–4.85 | 3.08–4.42 | 3.47–4.51 |
| $H_1$ (anomeric) | 4.70 | 4.98 | 4.60 | 4.72 |
| H-aromatic | — | 7.29 (2H, d, $J$ = 9.6 Hz, $H_8$), 7.75 (2H, d, $J$ = 6.8 Hz, $H_7$) | 6.35 (1H, d, $J$ = 7.2 Hz, $H_7$), 6.84 (1H, d, $J$ = 8.0 Hz, $H_8$), 7.54–7.64 (1H, m, $H_9$) | 7.16 (1H, d, $J$ = 9.6 Hz, $H_7$), 7.99 (1H, d, $J$ = 8.8 Hz, $H_9$), 8.11 (1H, d, $J$ = 7.6 Hz, $H_8$), 8.19 (1H, s, $H_{10}$) |
| –NH–CS–NH– | — | 7.47 ($H_9$), 10.66 ($H_{10}$) | 7.32 ($H_{10}$), 10.59 ($H_{11}$) | 7.79 ($H_{11}$), 11.21 ($H_{12}$) |

singlet signal at $\delta$ 14.05 ppm corresponds to the acidic proton of the trifluoroacetic acid (TFA) additive used to dissolve the polymer. The assignments align with the established structure of chitosan.

Moreover, Fig. 3b–d shows the spectra of the novel modified chitosan thiourea, including 4-fluoroaniline (**CHTUD1**), 2,4-difluoroaniline (**CHTUD2**), and 3-trifluoromethylaniline (**CHTUD3**). Crucially, the spectra revealed further signals that corroborate the effective grafting of the modified phenyl thiourea molecules. According to the chart of the **CHTUD1** sample, the establishment of the new thiourea (–NH–CS–NH–) function was clearly demonstrated by the emergence of two new, deshielded singlet signals that correspond to the two N–H protons (Fig. 3b). The NH proton ($H_9$) resonated at $\delta$ 7.47 ppm, whereas the less protected NH proton ($H_{10}$) emerged at $\delta$ 10.66 ppm. Conversely, the protons of the new thiourea (–NH–CS–NH–) function in the **CHTUD2** sample depicted at $\delta$ 7.32 ppm and 10.58 ppm related to the $H_{10}$ and $H_{11}$, respectively.[65] Meanwhile, the $^1$H NMR spectrum of the **CHTUD2** sample revealed the protons of the new thiourea at $\delta$ 7.79 and 11.21 ppm, owing to the $H_{11}$ and $H_{12}$, respectively (Fig. 3c). For the new aromatic protons in the **CHTUD1** sample, two multiplets in the aromatic region, which are typical of a 1,4-disubstituted (*para*) ring, showed the 4-fluorophenyl ring. Doublet signals displayed at $\delta$ 7.29 ppm ($H_7$, $J$ = 9.6 Hz) and other doublet signals at $\delta$ 7.75 ppm ($H_8$, $J$ = 6.8 Hz) are for the two pairs of aromatic protons. The three aromatic protons in the **CHTUD2** sample appeared as one doublet–doublet signal at $\delta$ 6.35 ppm, referring to the $H_7$ proton, and multiplet signals due to the $H_8$ and $H_9$ protons at $\delta$ 6.81–7.74 ppm, respectively. In contrast, the aromatic protons in the **CHTUD3** sample appeared as four signals, two doublet signals at $\delta$ 7.16 ppm & 7.99 ppm assigned for $H_7$ and $H_9$ protons, respectively, as well as a triplet signal due to the H8 proton displayed at $\delta$ 8.11 ppm ($J$ = 7.6 Hz), besides a singlet signal at $\delta$ 8.19 ppm assigned for the $H_{10}$ proton (Fig. 3d).[66] Meanwhile, the $^1$H NMR spectra of the three novel samples **CHTUD1**, **CHTUD2**, and **CHTUD3** exhibited the original signals of the chitosan backbone.

Lastly, the simultaneous detection of the native chitosan signals alongside the newly introduced aromatic and thiourea N–H signals validates the successful covalent synthesis of the target modified chitosan thiourea derivatives.

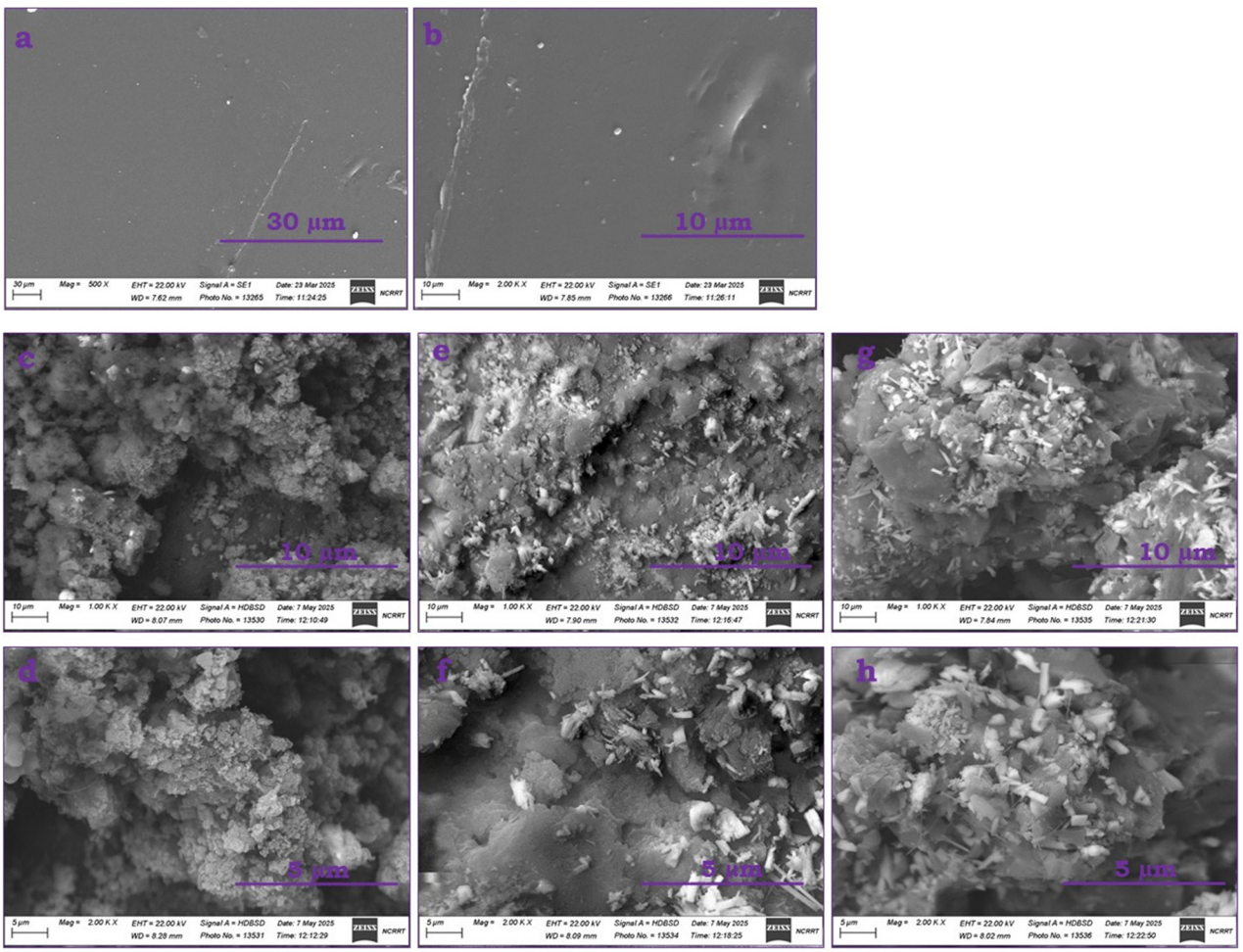


Fig. 4 SEM photos of the target samples at different magnifications: (a) chitosan at 500×, (b) chitosan at 2000×, (c) **CHTUD1** at 1000×, (d) **CHTUD1** at 2000×, (e) **CHTUD2** at 1000×, (f) **CHTUD2** at 2000×, (g) **CHTUD3** at 1000×, and (h) **CHTUD3** at 2000×.

**3.4.3. Surface morphology by scanning electron microscopy.** Fig. 4 shows the results of a comprehensive analysis of the surface morphological properties of native chitosan (**CH**) and its thiourea derivatives (**CHTUD1–3**) using scanning electron microscopy (SEM) at different magnifications (1000× and 2000×). The chemical incorporation of fluorinated aromatic moieties into the chitosan matrix *via* the thiourea function resulted in notable changes in surface topography. Frequently, with a magnification of 500×, the native chitosan seems uniform, smooth, and has a pretty uniform surface, as presented in Fig. 4a. Upon examination at a magnification of 2000× (Fig. 4b), the surface is unequivocally characterized as dense and devoid of porosity. The lack of visible pores, cracks, or substantial polymer aggregates suggests the development of a cohesive and dense polymer matrix.[67] This consistent, planar topography is indicative of chitosan films produced with the solvent-casting technique. The presence of strong intermolecular hydrogen bonds stabilizes the well-packed structure of the polymer chains, which in turn supports a uniform solvent evaporation process. Reduced gas and water vapor permeability and improved mechanical integrity are among the predicted attributes imparted by this thick, non-porous shape.[68]

Applying scanning electron microscopy (SEM) to the surface morphology of the modified chitosan-thiourea derivatives (**CHTUD1–3**) allowed us to examine the structural changes that occurred as a result of chemical alteration (Fig. 4c–h). A significant change in morphology is observed when compared to the initial chitosan film (previously illustrated in Fig. 4a and b, which exhibited a smooth, dense, and non-porous surface). In stark contrast, all micrographs of the modified derivatives at 1.00k× (Fig. 4c, e and g) and 2.00k× magnification (Fig. 4d, f and h) show a very uneven, rough, and heterogeneous surface. The smooth, film-like integrity that was there in the beginning has seen total disruption. Porosity, agglomerates, and shattered, coarse particles are now visible in the changed material (for example, see Fig. 4d and f).

Additionally, a notable new characteristic is the development of unique, separate microstructures. Fig. 4g and i illustrate that the rough polymer matrix is adorned with multiple bright, well-defined, rod-like or acicular crystalline structures. This drastic shift in shape from a smooth film to a rough, porous, and crystalline-containing matrix shows that there has been a significant change in both the chemical and structural makeup of the material. The alteration of the original compact polymer architecture is ascribed to the introduction of new thiourea functional groups, which disrupt the robust and orderly intermolecular hydrogen bonding present within the chitosan chains. The effective grafting of the thiourea derivative is directly visible in the form of the new crystalline phase.[69]

Previous investigations on modified chitosan derivatives based on fluorinated aromatic rings have shown that, in comparison to unmodified chitosan, the modified version exhibits surface roughness that is higher and microstructures that are more noticeable, confirming the microscopic level of structural modification.[70] The textured morphology has the capacity to enhance interactions and augment the surface area in applications, like antibacterial activity and drug delivery.[71]

**3.4.4. XRD analysis.** Fig. 5 reveals the X-ray diffraction (XRD) analysis of native **CH** as well as the modified chitosan thiourea derivatives (**CHTUD1–3**). As displayed in Fig. 5a, the

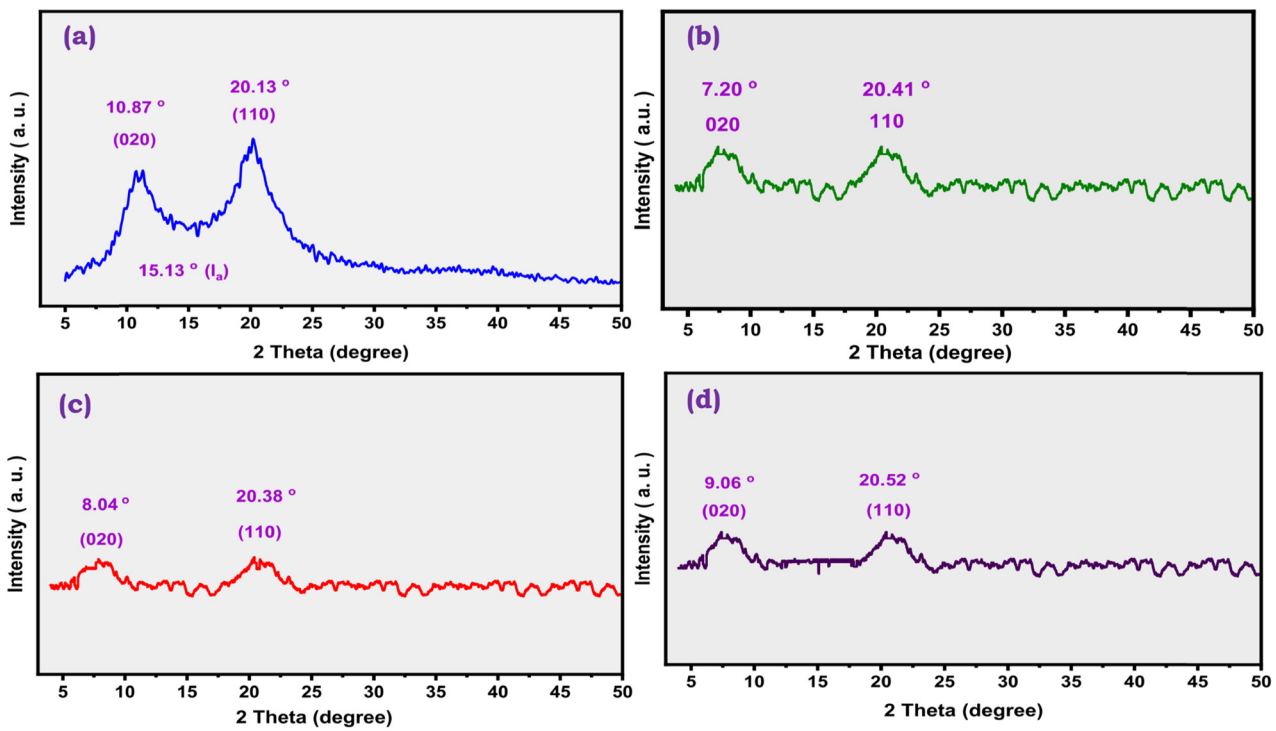


Fig. 5 X-ray diffraction patterns of (a) native **CH**, (b) modified **CHTUD1**, (c) modified **CHTUD2**, and (d) modified **CHTUD3**.

XRD chart of the native chitosan displayed a semicrystalline structure, characterized by two distinct reflections at $2\theta$ = 10.87° (020 plane) and 20.13° (110 plane).[72] In addition, the "tendon" form is characterized by the (020) reflection at $2\theta$ = 10.87° ($d$-spacing = 8.09 Å), which indicates that the native chitosan (**CH**) exhibited hydrated polymorphism in its X-ray diffraction pattern.[73] Significant structural changes occurred upon modification of the native chitosan into fluorinated chitosan thiourea derivatives (**CHTUD1–3**). The 020-plane reflection at $2\theta$ = 10.87° was absent in all modified samples, indicating a significant alteration of the original crystal structure (Fig. 5b–d). Conversely, the modified chitosan thiourea samples demonstrated a new distinct peak at $2\theta$ = 7.20° (**CHTUD1** sample), 8.04° (**CHTUD2** sample), and 9.06° (**CHTUD3** sample). It is noteworthy that the intensity of the characteristic peak diminished because of the incorporated fluorinated thiourea moiety. Using eqn (3), the crystallinity index value of the native chitosan was calculated to be 72.12%, which declined to 53.44%, 53.13%, and 50.88% for **CHTUD1**, **CHTUD2**, and **CHTUD3**, respectively. The consumption of the amino group in the chitosan structure during its conversion into isothiocyanate and subsequent combination with fluorinated amines results in the formation of thiourea, which reduces the crystallinity of the biopolymer, producing amorphous or less crystalline samples. Several variables, including hydrophobic forces, steric hindrance, and π–π stacking interactions, are expected to influence this transition. These interactions have the potential to increase the appropriateness of these derivatives for use in biological applications.

**3.4.5. TGA analysis.** Thermogravimetry/derivative thermogravimetry (TGA/DTG) was employed across a temperature range of 30–700 °C to investigate the thermal properties of native **CH** and the fluorinated chitosan thiourea derivatives (**CHTUD1–3**). As displayed in Fig. 6, the initial degradation step commenced at around 30 °C, associated with the loss of adsorbed moisture, highlighting significant differences between the unmodified polymer (**CH**) and its thiourea derivatives (**CHTUD1–3**). Unmodified **CH** displayed a major degradation peak at 102.45 °C, corresponding to a moisture-related weight loss of 13.09% (Fig. 6a). In sharp contrast, all the modified samples (**CHTUD1**, **CHTUD2**, and **CHTUD3**) exhibited their degradation peaks at a mean temperature of 60 °C. This thermal shift was accompanied by a progressive and substantial reduction in moisture-related weight loss, which was recorded at 2.99%, 3.58%, and 3.99%, respectively. The reduction in moisture content and the transition to elevated temperature peaks primarily result from the insertion of fluorinated aromatic thiourea functions into the **CH** backbone, which diminishes the polymer's hydrophilicity by introducing more hydrophobic moieties (Fig. 6b–d). Derivatives also have a greater moisture loss temperature, which might mean that the residual water molecules are more tightly bonded to the polymer matrix or are less accessible.

Conversely, fluorinated chitosan thiourea (**CHTUD1–3**) demonstrates superior thermal stability compared to CH, with the

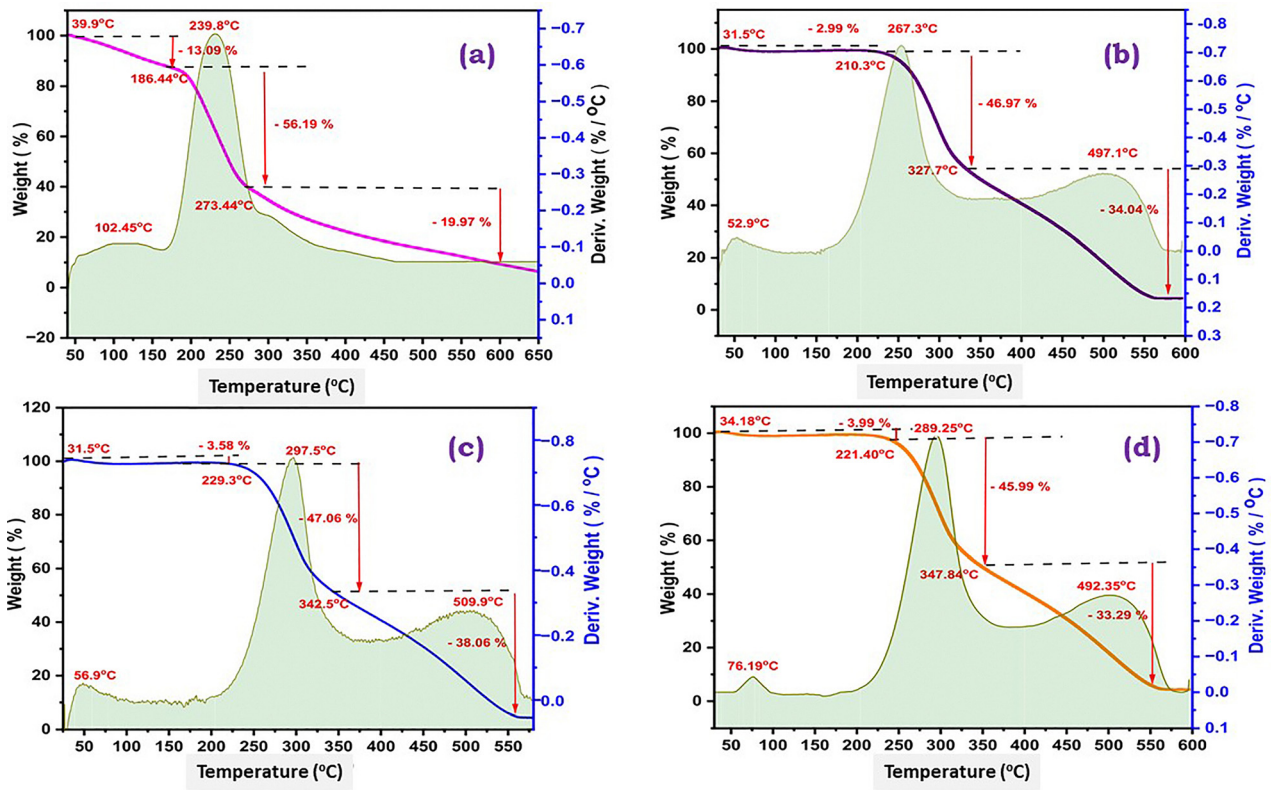


Fig. 6 TGA/DTG curves of (a) native chitosan, (b) the **CHTUD1** sample, (c) the **CHTUD2** sample, and (d) the **CHTUD3** sample.

Table 5 Zone of inhibition of chitosan, chitosan isothiocyanate and modified fluorinated-chitosan derivatives (**CHTUD1–3**) compared with positive control drugs

| | Gram-positive bacteria | | Gram-negative bacteria | | Fungi |
|---|---|---|---|---|---|
| Cpd no. | *B. subtilis* (ATCC 6633) | *S. aureus* (ATCC 6538) | *K. pneumoniae* (ATCC 13883) | *S. typhi* (ATCC 6539) | *C. albicans* (ATCC 10221) |
| **CH** | 25 ± 12 | 27 ± 20 | 17 ± 18 | 20 ± 21 | 23 ± 12 |
| **CHTUD1** | 28 ± 17 | 32 ± 18 | 19 ± 23 | 22 ± 19 | 28 ± 13 |
| **CHTUD2** | 35 ± 11 | 32 ± 12 | 20 ± 10 | 21 ± 28 | 28 ± 16 |
| **CHTUD3** | 32 ± 17 | 33 ± 16 | 21 ± 24 | 24 ± 13 | 30 ± 12 |
| **AMP** | 25 ± 10 | 31 ± 25 | 20 ± 18 | 22 ± 16 | — |
| **NYS** | — | — | — | — | 22 ± 17 |

**AMP** = ampicillin; **NYS** = nystatin.

second degradation step occurring in **CHTUD1** within the range of 210.3–327.7 °C, **CHTUD2** within 229.3–342.5 °C, and **CHTUD3** within 221.40–347.4 °C. At this stage, the weight loss of fluorinated chitosan thiourea is approximately ∼45%, which is lower than that of unmodified chitosan (56%). This finding provides support for the notion that fluorinated chitosan thiourea exhibits greater thermal stability compared to pristine chitosan.[74] Also, the second stage of the three samples is compatible with the degree of substitution assessment, in that the order of thermal stability is **CHTUD2** > **CHTUD1** > **CHTUD3** > **CH** (Fig. 6).

Continuously, thermal degradation analysis of the third stage indicates that the chitosan thiourea derivatives exhibit significant alteration from the unmodified form of chitosan. Between 273.44 and 600 °C, unmodified chitosan undergoes its third degradation phase, resulting in a weight loss of approximately 19.97% (Fig. 6a). This step, most likely involved with the breakdown of cross-linked structures from chitosan's amino groups, leaves a 10.75% residual weight at 600 °C, suggesting little incomplete decomposition. While the chitosan thiourea derivatives (**CHTUD1–3**) exhibit elevated temperatures compared to those of native chitosan. The third degradation phase initiates at elevated temperatures, commencing at 327 °C (**CHTUD1**), 342 °C (**CHTUD2**), and 347 °C (**CHTUD3**). Dehydration, thiourea bond breaking, aromatic ring elimination, and possible depolymerization are all components of this first degradation step in the derivatives.[75] In addition, the $T_{50}$ value quantifies this enhanced stability, representing the temperature at which a sample loses 50% of its weight.[76] So, the $T_{50}$ of untreated chitosan was measured at 250 °C, while the thiourea derivatives exhibited significantly elevated values: 341 °C (**CHTUD1**), 322 °C (**CHTUD2**), and 336 °C (**CHTUD3**). Collectively, both the delayed onset of third-stage degradation and the dramatically increased $T_{50}$ values confirm that the chitosan thiourea derivatives possess significantly greater thermal stability than the original chitosan. This observation provides strong evidence for the successful formation of the target modified polymer. As a result, this superior thermal stability is a vital feature, positioning these materials for high-performance applications, such as biomedical implants or wound dressings, that must endure prolonged exposure to heat.

### 3.5. Antimicrobial activity

**3.5.1. *In vitro* antimicrobial activity.** To evaluate the sensitivity of the modified fluorinated-thiourea chitosan derivatives **CHTUD1–3** and native chitosan (**CH**) toward antimicrobial activity, we tested two Gram-positive bacteria, [*B. subtilis* (ATCC 6633) and *S. aureus* (ATCC 6538)], two Gram-negative bacteria, [*K. pneumoniae* (ATCC 13883) and *S. typhi* (ATCC 6539)], and one fungal strain, [*C. albicans* (ATCC 10221)]. The antimicrobial effectiveness of the derivatives was assessed against these microbial strains, with the results expressed as zones of inhibition (ZI) in millimeters (mm) using the agar well diffusion method at 50 mg $mL^{-1}$ for the samples and 10 mg $mL^{-1}$ for the positive control, representing the average of three measurements, as shown in Table 5. Ampicillin and nystatin were utilized as positive control agents to establish a benchmark for the observed *in vitro* antimicrobial activity, rather than to suggest equivalent pharmacological efficacy.

The synthesized fluorinated-thiourea chitosan derivatives **CHTUD1–3** demonstrated significant antimicrobial activity, with zones of inhibition ranging from 28 ± 17 to 35 ± 11 mm against *B. subtilis* (ATCC 6633) and from 32 ± 12 to 33 ± 16 mm against *S. aureus*. In comparison, the unmodified chitosan exhibited zones of inhibition of 25 ± 12 and 27 ± 20 mm, while ampicillin displayed zones of inhibition of 25 ± 10 and 31 ± 25 mm against the same strains. Conversely, the thiourea chitosan derivatives **CHTUD1–3** exhibited moderate activity, with zones of inhibition ranging from 19 ± 23 to 21 ± 24 mm against *K. pneumoniae* (ATCC 13883) and from 21 ± 28 to 24 ± 13 mm against *S. typhi* (ATCC 6539). This was in comparison to ampicillin, which had zones of inhibition of 20 ± 18 and 22 ± 16 mm, and unmodified chitosan, which showed zones of inhibition of 17 ± 18 and 20 ± 21 mm against the same strains. Furthermore, the modified thiourea-chitosan derivatives exhibited enhanced antifungal activity, with zones of inhibition measuring 28 ± 13 mm, 28 ± 16 mm, and 30 ± 12 mm for **CHTUD1**, **CHTUD2**, and **CHTUD3**, respectively. This contrasted with unmodified chitosan, which had an inhibition zone of 23 ± 12 mm, and nystatin, which had an inhibition zone of 22 ± 17 mm.

**3.5.2. Evaluation of the inhibitory concentrations and structure–activity relationship (SAR).** The fluorinated-thiourea chitosan derivatives **CHTUD1–3** were evaluated for their antibacterial activity by determining the minimum inhibitory concentration (MIC) that prevents microorganism growth by the broth microdilution method as described previously.[77,78] The obtained data represent the MIC values of the designed chitosan derivatives compared to native chitosan and positive

control drugs (ampicillin and nystatin) and are represented in Table 6 and expressed in μg $mL^{-1}$.

Initially, the modification of chitosan with fluorinated thiourea derivatives demonstrated considerable antimicrobial activity when compared to native chitosan, suggesting that the introduction of a thiourea linker and hydrophobic substituted-phenyl groups enhances antimicrobial efficacy. Among the synthesized derivatives, the incorporation of the 2,4-difluorophenylthiourea moiety into chitosan, as represented in compound **CHTUD2**, revealed promising activity, with MIC values of 7.8, 7.8, 15.62, and 15.62 μg $mL^{-1}$ against *B. subtilis*, *S. aureus*, *K. pneumoniae*, and *C. albicans*, respectively, comparable to ampicillin. Conversely, compound **CHTUD2** demonstrated moderate activity against *S. typhi* with an MIC value of 62.5 μg $mL^{-1}$, which is more potent than that of native chitosan (MIC = 125 μg $mL^{-1}$), but still less effective than ampicillin (MIC = 15.62 μg $mL^{-1}$). This enhanced activity can be attributed to the presence of two fluorinated groups at the 2 and 4 positions of the phenyl ring, which may contribute to increased lipophilicity and membrane penetration, or may enhance binding affinity to biological targets. Additionally, the presence of fluorinated groups in the *ortho* and *para* positions contributes to the stability of the aromatic ring system by repelling electron density toward the fluorinated groups due to their high electronegativity. Furthermore, the conjugation of 4-fluorophenylthiourea with chitosan to form compound **CHTUD1** exhibited significant activity against *S. aureus* with an MIC value of 7.8 μg $mL^{-1}$, equivalent to that of ampicillin, while displaying MIC values of 31.25 μg $mL^{-1}$ against *B. subtilis*, *K. pneumoniae*, and *S. typhi*. On the other hand, compound **CHTUD3**, which involved the incorporation of 3-(trifluoromethyl)phenyl thiourea into chitosan, demonstrated potent antibacterial activity against *S. aureus* and *S. typhi*, with MIC values of 7.8 and 15.62 μg $mL^{-1}$, respectively. Compound **CHTUD3** exhibited enhanced antibacterial activity relative to native chitosan; however, it did not show a significant improvement in antibacterial efficacy when compared to ampicillin.

The synthesized chitosan thiourea derivatives, designated as **CHTUD1–3**, demonstrated noteworthy antifungal activity, with an MIC value of 15.62 μg $mL^{-1}$. In contrast, native chitosan displayed an MIC of 62.5 μg $mL^{-1}$.

The structure–activity relationship (SAR) analysis demonstrates that the introduction of fluorinated groups can enhance antimicrobial activity, particularly when these groups are positioned at the *ortho* and *para* locations on the aromatic ring. This enhancement can be attributed to the high

Table 6 Minimum inhibitory concentrations (MICs) of chitosan, chitosan isothiocyanate and modified fluorinated-chitosan derivatives (**CHTUD1–3**) in comparison to positive control drugs

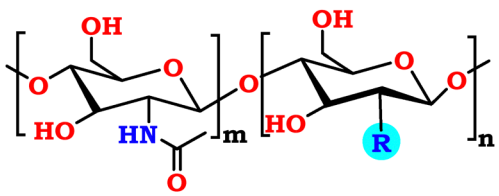


| | | Anti-microbial activity expressed as MIC values represented by μg $mL^{-1}$ | | | | |
|---|---|---|---|---|---|---|
| | | Gram-positive bacteria | | Gram-negative bacteria | | Fungi |
| Cpd no. | R | *B. subtilis* (ATCC 6633) | *S. aureus* (ATCC 6538) | *K. pneumoniae* (ATCC 13883) | *S. typhi* (ATCC 6539) | *C. albicans* (ATCC 10221) |
| **CH** | $-NH_2$ | 62.5 | 62.5 | 125 | 125 | 62.5 |
| **CHTUD1** | 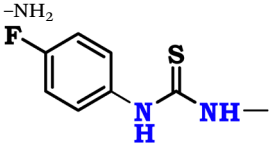 | 31.25 | 7.8 | 31.25 | 31.25 | 15.62 |
| **CHTUD2** | 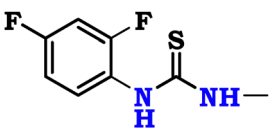 | 7.8 | 7.8 | 15.62 | 62.5 | 15.62 |
| **CHTUD3** | 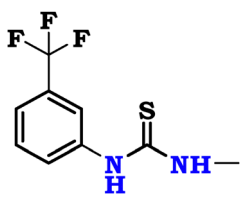 | 15.62 | 7.8 | 31.25 | 15.62 | 15.62 |
| **AMP** | | 7.8 | 7.8 | 15.62 | 15.62 | — |
| **NYS** | | — | — | — | — | 7.8 |

**AMP** = ampicillin; **NYS** = nystatin.

Table 7 Minimum bactericidal and fungicidal concentrations (MBCs/MFCs) of chitosan, chitosan isothiocyanate and modified fluorinated-chitosan derivatives (**CHTUD1–3**) in comparison to positive control drugs

| | Anti-microbial activity expressed as MBC/MFC values represented by μg mL$^{-1}$ | | | | | | | | | |
|---|---|---|---|---|---|---|---|---|---|---|
| | Gram-positive bacteria | | | | Gram-negative bacteria | | | | Fungi | |
| | *B. subtilis* (ATCC 6633) | | *S. aureus* (ATCC 6538) | | *K. pneumoniae* (ATCC 13883) | | *S. typhi* (ATCC 6539) | | *C. albicans* (ATCC 10221) | |
| Cpd no. | MBC | Ratio | MBC | Ratio | MBC | Ratio | MBC | Ratio | MFC | Ratio |
| **CH** | 125 | 2 | 125 | 2 | 250 | 2 | 500 | 4 | 250 | 4 |
| **CHTUD1** | 62.5 | 2 | 15.62 | 2 | 62.5 | 2 | 62.5 | 2 | 15.62 | 1 |
| **CHTUD2** | 15.62 | 2 | 15.62 | 2 | 31.25 | 2 | 62.5 | 1 | 15.62 | 1 |
| **CHTUD3** | 15.62 | 1 | 15.62 | 2 | 62.5 | 2 | 31.25 | 2 | 31.25 | 2 |
| **AMP** | 7.8 | 1 | 7.8 | 1 | 31.25 | 2 | 31.25 | 2 | — | — |
| **NYS** | — | | — | | — | | — | | 15.62 | 2 |

**AMP** = ampicillin; **NYS** = nystatin.

electronegativity of the fluorine atom, which exerts an inductive (–I) effect that withdraws electron density from the aromatic phenyl ring. Consequently, an increase in the number of fluorine atoms results in a greater electron-withdrawing effect, thereby stabilizing the aromatic system and improving the overall antimicrobial efficacy of the compounds. Furthermore, the incorporation of fluorine atoms increases lipophilicity, facilitating membrane penetration and, subsequently, enhancing bioavailability. Moreover, for compound **CHTUD3**, which possesses a trifluoromethyl group at the *meta* position, its activity primarily arises from the lipophilicity of the fluorine atom, while the presence of this group in the *meta* position does not enhance the stability of the phenyl ring.

**3.5.3. Bactericidal and fungicidal activity.** To determine the biocidal activity, our work was extended to evaluate the minimum bactericidal concentration (MBC) and minimum fungicidal concentration (MFC) of the modified chitosan derivatives in comparison to native chitosan. Notably, all modified fluorinated thiourea–chitosan derivatives, designated as **CHTUD1–3**, exhibited MBC values ranging from 15.62 to 62.5 μg mL$^{-1}$ and MFC values from 15.62 to 31.25 μg mL$^{-1}$. In contrast, native chitosan demonstrated MBC values between 125 and 500 μg mL$^{-1}$ and MFC of 250 μg mL$^{-1}$ (Table 7).

Regarding the efficacy of modified chitosan against *B. subtilis*, **CHTUD2** and **CHTUD3** exhibited MBC values of 15.62 μg mL$^{-1}$, indicating a slightly lower bactericidal effect than ampicillin but a higher potency than **CHTUD1**, which had an MBC of 62.5 μg mL$^{-1}$. Furthermore, the modified chitosan derivatives **CHTUD1–3** displayed equipotent bactericidal activity against *S. aureus* with MBC values of 15.62 μg mL$^{-1}$. Conversely, the modified thiourea chitosan derivatives **CHTUD1–3** showed low sensitivity and exhibited bactericidal activity against Gram-negative bacterial strains, with MBC values ranging from 31.25 to 62.5 μg mL$^{-1}$ for the tested strains. Moreover, **CHTUD2** demonstrated an MBC value of 31.25 μg mL$^{-1}$ against *K. pneumoniae*, which is equivalent to that of ampicillin. Additionally, **CHTUD3** exhibited an identical MBC of 31.25 μg mL$^{-1}$ against *S. typhi*, also comparable to ampicillin.

In terms of antifungal activity, **CHTUD3** demonstrated an MFC value of 31.25 μg mL$^{-1}$, which was two-fold less active than **CHTUD1** and **CHTUD2**, both exhibiting MFC values of 15.62 μg mL$^{-1}$, equipotent to nystatin; however, all derivatives retained fungicidal properties. It has been previously reported that the MBC/MIC ratio was approximately 4, suggesting that the synthesized derivatives exhibited bactericidal properties rather than bacteriostatic ones.[79] Based on the obtained results and the determined ratio, we concluded that all derivatives demonstrated both bactericidal and fungicidal activity.

In conclusion, the synthesized fluorinated thiourea chitosan derivatives **CHTUD1–3** exhibited significant bactericidal and fungicidal properties, evidenced by reduced MBC and MFC. In certain instances, these derivatives demonstrated equipotent activity when compared to established positive control drugs.

**3.5.4. Biofilm inhibitory activity.** Microorganisms adhere and aggregate to form biofilms, which are encased in a layer of polysaccharide-rich extracellular matrix.[80] Compared to planktonic cells, biofilms offer numerous advantages, primarily due to their increased resistance to adverse environmental conditions.[81] This inherent resilience complicates the

Table 8 Biofilm inhibitory activity of modified fluorinated chitosan derivatives **CHTUD1–3** represented by percentage at different concentrations from MBCs

| | Anti-biofilm activity % | | | | | |
|---|---|---|---|---|---|---|
| | *S. aureus* (ATCC 6538) | | | *S. typhi* (ATCC 6539) | | |
| Cpd no. | 75% MBC | 50% MBC | 25% MBC | 75% MBC | 50% MBC | 25% MBC |
| **CH** | 90.76 ± 0.005 | 69.37 ± 0.003 | 24.30 ± 0.003 | 90.39 ± 0.003 | 73.50 ± 0.001 | 51.24 ± 0.005 |
| **CHTUD1** | 96.36 ± 0.002 | 81.84 ± 0.007 | 72.74 ± 0.003 | 93.06 ± 0.005 | 81.85 ± 0.003 | 74.31 ± 0.002 |
| **CHTUD2** | 92.84 ± 0.002 | 73.15 ± 0.006 | 61.27 ± 0.005 | 91.70 ± 0.004 | 77.55 ± 0.003 | 68.49 ± 0.004 |
| **CHTUD3** | 95.22 ± 0.005 | 82.04 ± 0.007 | 72.87 ± 0.003 | 93.80 ± 0.005 | 83.16 ± 0.008 | 76.27 ± 0.003 |

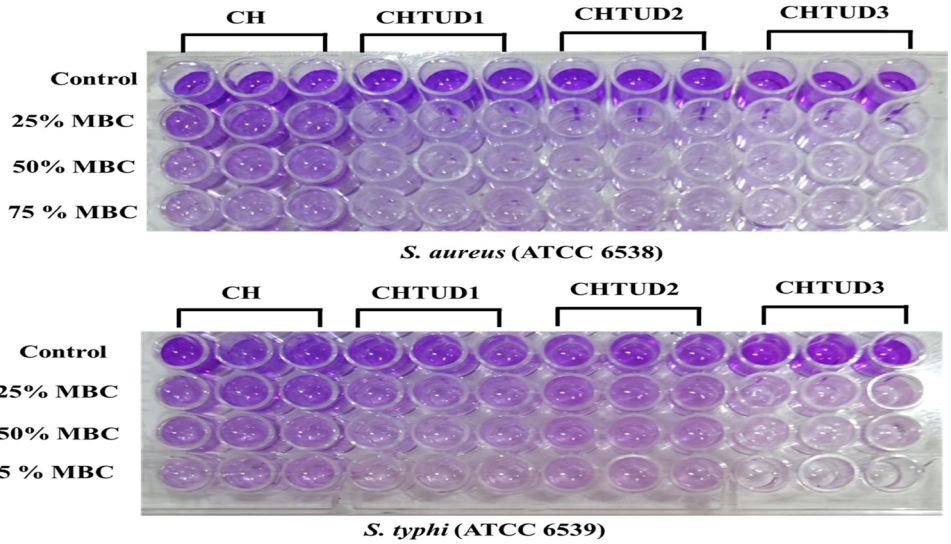


Fig. 7 Biofilm inhibitory activity of modified fluorinated chitosan derivatives **CHTUD 1–3**.

eradication of biofilms, necessitating agents with strong anti-biofilm properties. Typically, effective antibacterial agents demonstrate robust activity against biofilm structures. This study aims to investigate the efficacy of fluorinated thiourea chitosan derivatives **CHTUD1–3** by assessing their anti-biofilm properties at various concentrations from MBC levels (75, 50, and 25%) using a microtiter plate assay as described previously[51] against *S. aureus* (ATCC 6538) and *S. typhi* (ATCC 6539).

According to Table 8, all tested modified fluorinated chitosan derivatives **CHTUD1–3** exhibited remarkable antibiofilm activity against *S. aureus* and *S. typhi*. The inhibition percentage increased with the concentration of the tested compounds, indicating a dose-dependent response. Notably, the modified **CHTUD1** and **CHTUD3** demonstrated the highest biofilm inhibitory concentrations, with their inhibitory percentages being approximately 1–2% higher at all concentrations compared to **CHTUD2**. However, all modified **CHTUD1–3** exhibited greater biofilm activity than native chitosan. At high concentrations (75% MBC), all modified chitosans **CHTUD1–3** revealed biofilm inhibitory activities exceeding 90% (IBP = 92.84 ± 0.002–96.36 ± 0.002%) against *S. aureus* and (IBP = 91.70 ± 0.004–93.80 ± 0.005%) against *S. typhi*.

At low concentrations (25% MBC), the modified fluorinated chitosan derivatives **CHTUD 1–3** demonstrated inhibitory percentages ranging from (IBP = 61.27 ± 0.005–72.87 ± 0.003%) against *S. aureus* to (IBP = 68.49 ± 0.004–76.27 ± 0.003%) against *S. typhi*. In contrast, native chitosan showed biofilm inhibitory activities of 24.30 ± 0.003% against *S. aureus* and 51.24 ± 0.005% against *S. typhi* (Fig. 7). This indicates that the modification of chitosan with fluorinated thiourea enhances antibiofilm formation due to increased hydrophobicity and strong electrostatic interactions between the positively charged chitosan backbone and the negatively charged bacterial cell surfaces. Additionally, the presence of fluorinated substituents may influence surface energy and membrane permeability, leading to better adhesion to bacterial biofilms and enhanced bactericidal effects.

**3.5.5. *In silico* toxicity prediction.** Toxicity prediction is a crucial tool in drug development and medicinal chemistry. It is essential for minimizing costs, reducing the number of experimental assays, and identifying the most promising and safe candidates for advancement.[82] By utilizing accurate *in silico* toxicity evaluations, researchers can improve efficiency, ensure safety, and accelerate the drug discovery process by early identification of potential adverse effects.[52,83] The toxicity prediction for the modified fluorinated-thiourea chitosan derivatives **CHTUD1–3**, compared to native chitosan (**CH**), was conducted using the ProtexIII web tool as described previously.[84,85]

Fig. 8 illustrates the toxicity profile of the evaluated derivatives, demonstrating that the designed fluorinated-thiourea chitosan derivatives **CHTUD1–3** exhibited non-nutritional

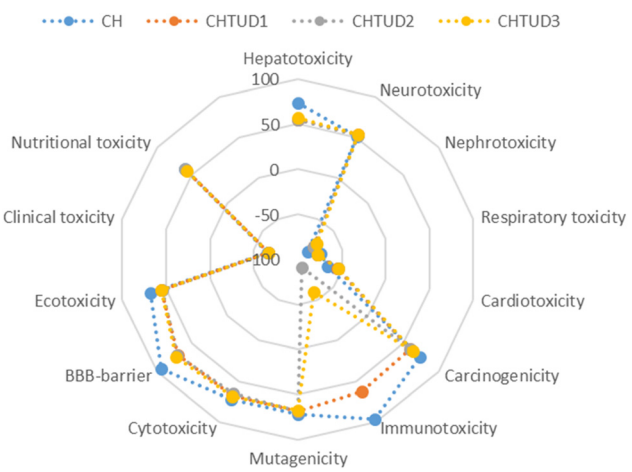


Fig. 8 *In silico* toxicity prediction chart for the modified fluorinated thiourea chitosan derivatives **CHTUD1–3** and native chitosan.

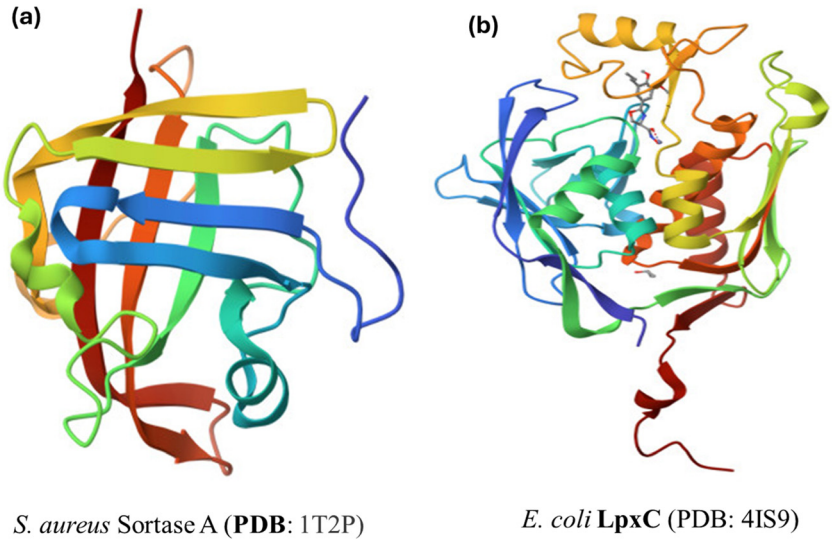


Fig. 9 3D structure of two target enzymes: (a) *S. aureus* sortase A (PDB: 1T2P) and (b) *E. coli* LpxC (PDB: 4IS9).

toxicity, non-ecotoxicity, and non-BBB-barrier toxicity, with commendable probability values ranging from 54% to 73%. Furthermore, these derivatives were anticipated to demonstrate no toxicity concerning cytotoxicity, mutagenicity, and carcinogenicity. However, **CHTUD2** and **CHTUD3** displayed immunotoxin characteristics with probability values of 90% and 60%,

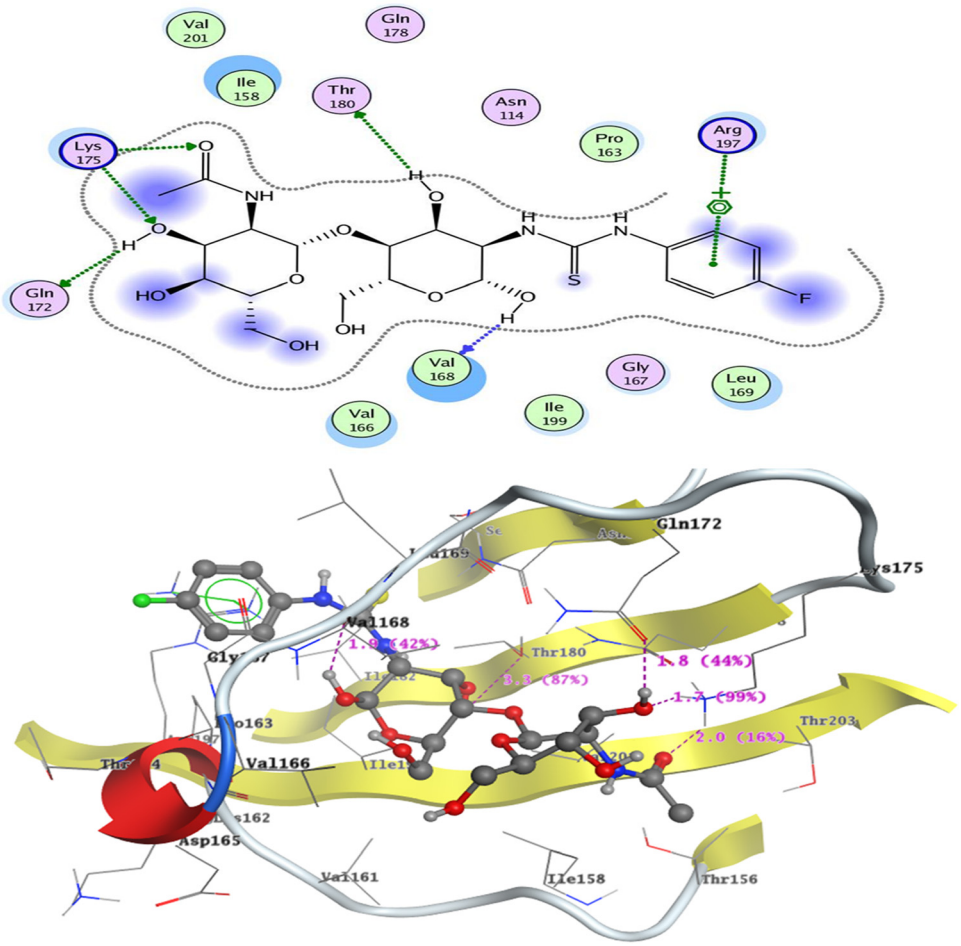


Fig. 10 2D and 3D docking conformation of **CHTUD1** inside the active site of sortase A (PDB: 1T2P).

respectively; this observation may be attributed to the increased number of fluorinated atoms in their molecular structure. Additionally, all modified derivatives, along with native chitosan, were predicted to possess toxicity related to nephrotoxicity, cardiotoxicity, and respiratory toxicity, exhibiting moderate percentage values. Moreover, the tested derivatives were forecasted to exhibit clinical toxicity with a probability of 66%, compared to native chitosan, which had a probability of 65%. Notably, the application of these derivatives as antimicrobial agents, with potential for biofilm formation, was predicted to be safe regarding hepatotoxicity and neurotoxicity, with favorable probability values.

**3.5.6. *In silico* molecular docking simulation.** The docking simulation was performed on the active sites of sortase A (SrtA) in *S. aureus*, a Gram-positive bacterium that helps anchor surface adhesins to the cell wall, where inhibiting sortase A has been shown to disrupt adhesion and biofilm formation.[86,87] For the Gram-negative strain (*S. typhi*), we focused on LpxC, an enzyme crucial for lipid A biosynthesis in the outer membrane, where inhibiting LpxC alters the outer membrane, thereby preventing biofilm formation (Fig. 9).[88] The docking simulation was conducted on the following 3D structures of the following enzymes: sortase A (PDB: 1T2P) (https://www.rcsb.org/structure/1T2P; last accessed on 22/10/2025) and LpxC (PDB: 4IS9) (https://www.rcsb.org/structure/4IS9; last accessed 22/10/2025).

Regarding the docking results of the designed compounds inside *S. aureus* sortase A (PDB: 1T2P), we found that the first derivative, the 4-fluorophenylthiourea chitosan derivative **CHTUD1**, exhibited a binding affinity of −17.59 kcal mol$^{-1}$. The residue Lys175 interacted with **CHTUD1**, forming two hydrogen bonds: one with the oxygen of the carbonyl related to the acetyl group of the *N*-acetyl glucosamine ring (Glu-Nac) and another with the oxygen of the hydroxyl group at C3 of *N*-acetyl glucosamine. The bond lengths were 2.0 Å and 1.7 Å, with strengths of 16% and 99%, respectively. Furthermore, the hydroxyl group also interacted with Gln172, exhibiting a bond length of 1.8 Å and a strength of 44%. For the glucosamine ring (Glu-N), the residues Val168 and Thr180 interacted, forming hydrogen bond donors with the hydroxyl groups at C1 and C3, with bond lengths of 1.9 Å and 3.3 Å, respectively. Additionally, to confirm the stability of the complex, a new arene–cation interaction was observed between the phenyl group of the thiourea derivative and Arg157 (Fig. 10).

The second thiourea chitosan derivative, **CHTUD2**, exhibited a predicted binding affinity of −18.55 kcal mol$^{-1}$, forming seven hydrogen bonds. These bonds are distributed throughout the compound, with four hydrogen bonds involving the

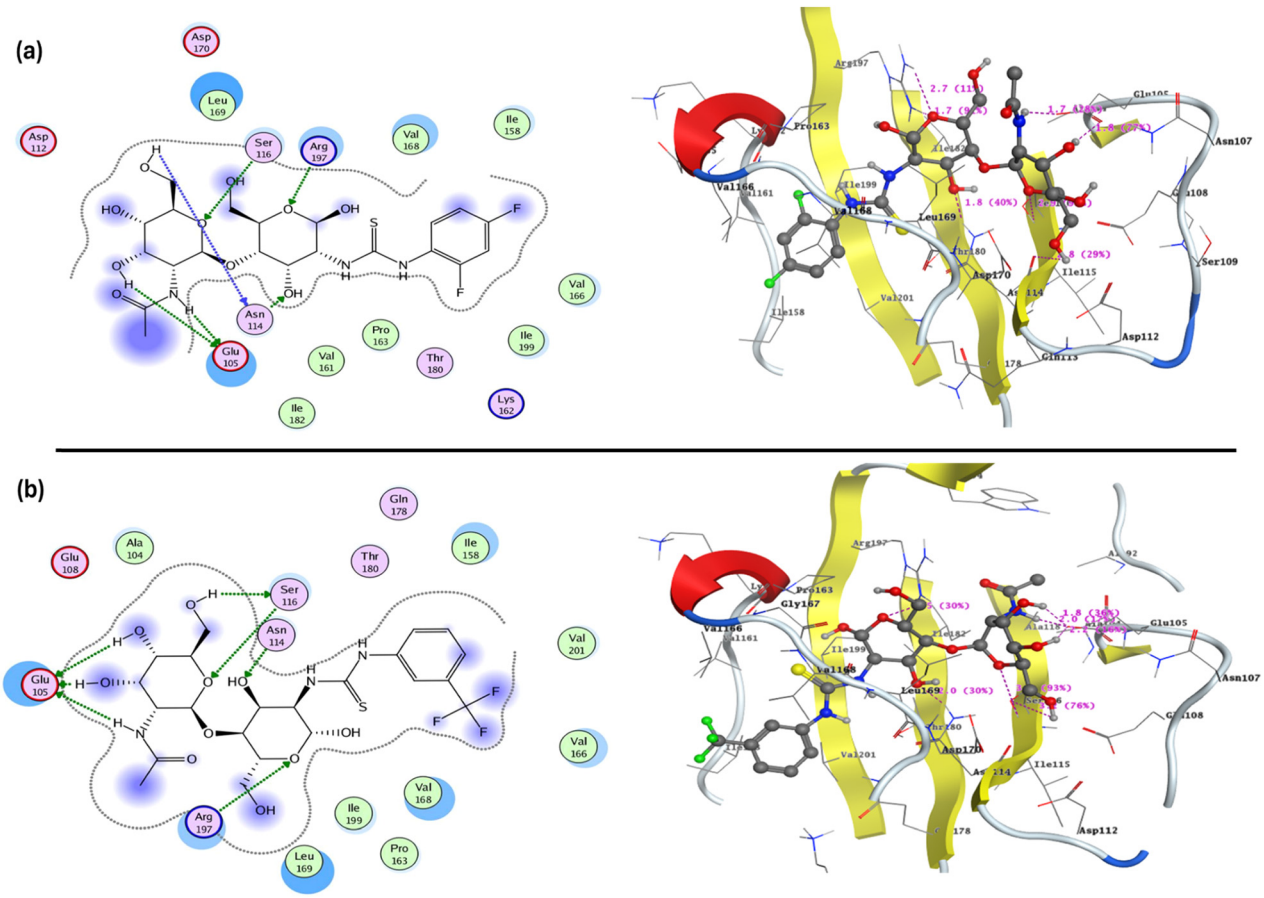


Fig. 11 2D and 3D docking conformation of (a) **CHTUD2** and (b) **CHTUD3** inside the active site of sortase A (PDB: 1T2P).

*N*-acetyl glucosamine ring (Glu-Nac). Two of these bonds act as sidechain donors between Glu105 and the NH of the acetyl group, as well as the hydroxyl group at C3 of the Glu-Nac, with bond lengths of 1.7 and 1.8 Å and strengths of 28 and 77%, respectively. Meanwhile, the hydroxyl group at C6 of the Glu-Nac serves as a backbone donor for a hydrogen bond with Asn114, with a bond length of 2.8 Å.[89] Additionally, the oxygen in the pyranose ring acts as a hydrogen bond acceptor for Ser116, with a bond length of 2.9 Å and a strength of 98%. Furthermore, the glucosamine ring (Glu-N) forms two hydrogen bond acceptors with Arg197 and the oxygen of the pyranose ring, with bond lengths of 1.7 and 2.7 Å. The hydroxyl group at C3 of the glucosamine ring (Glu-N) also creates a hydrogen bond with Asn114, measuring 1.8 Å in length and exhibiting a strength of 40%. All of these interactions are illustrated in Fig. 11a, where the conformation of **CHTUD2** also indicates a hydrophobic interaction, represented as a blue shadow region over the 2,4-difluorophenyl group of the thiourea derivative and the acetyl group.

Conversely, the **CHTUD3** molecule was docked into the active site of *S. aureus* sortase A (PDB: 1T2P), revealing a binding affinity of −16.41 kcal mol$^{-1}$, with four hydrogen bond donors and three hydrogen bond acceptors. To summarize and highlight the key groups in **CHTUD3** that interact with the binding pocket, a visualization analysis was conducted to explore the relationship between these interactions and the observed binding affinities. The **CHTUD3** demonstrated a binding affinity of −16.41 kcal mol$^{-1}$. The interaction involved two pyranose rings: the glucosamine ring (Glu-N) and the *N*-acetylglucosamine ring (Glu-Nac). Initially, the acidic amino acid Glu105 bound to the hydroxyl groups at C3 and C4, as well as the NH group of the *N*-acetyl glucosamine ring (Glu-Nac), with bond lengths of 2.2, 1.8, and 2.0 Å, and strengths of 16%, 36%, and 17%, respectively, acting as three hydrogen bond

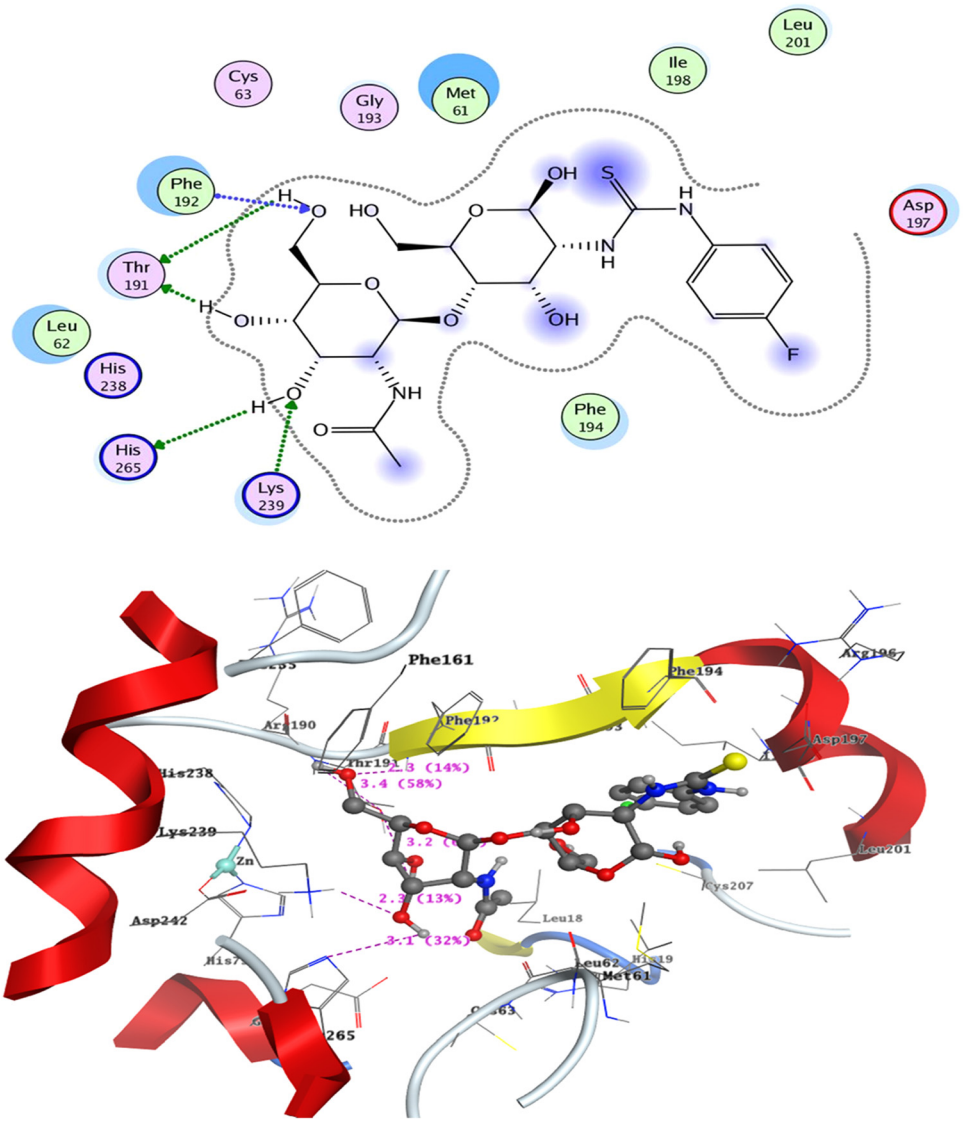


Fig. 12 2D and 3D docking conformation of **CHTUD1** inside the active site of LpxC (PDB: 4IS9).

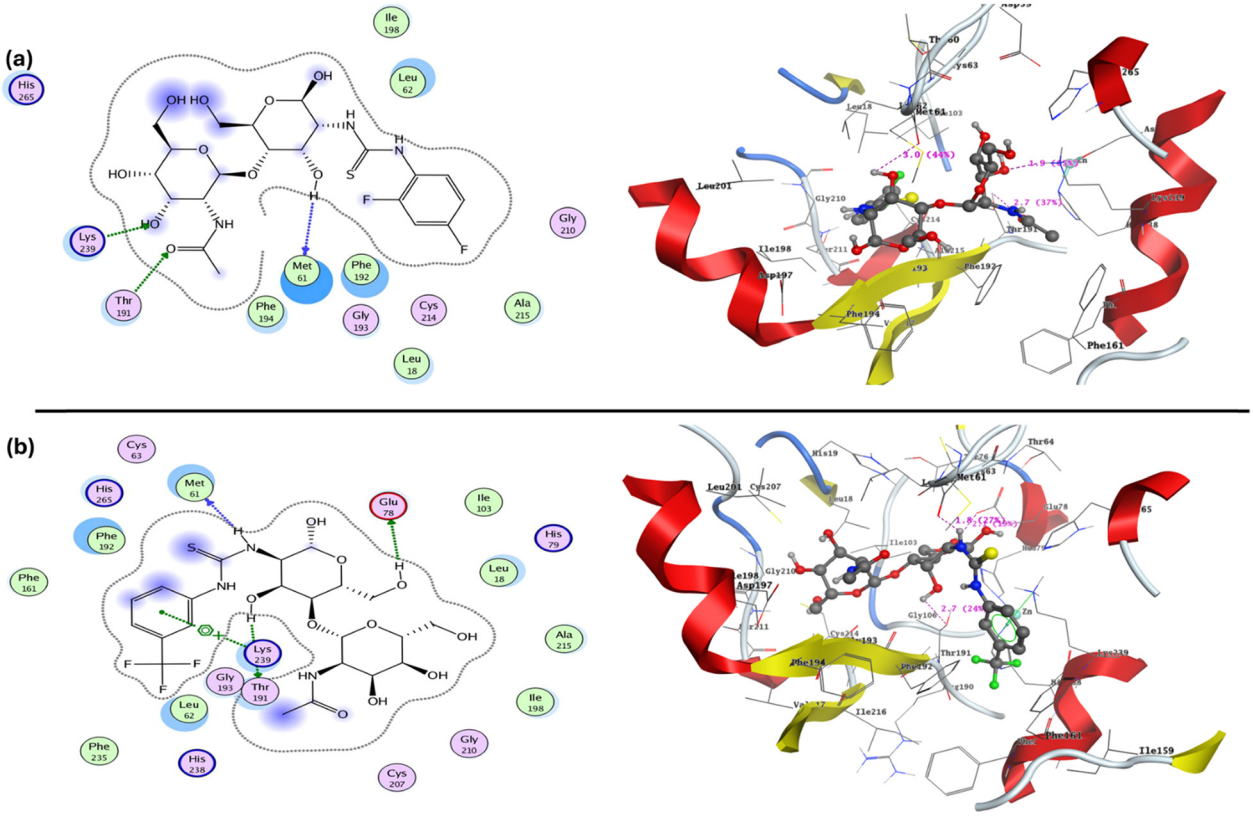


Fig. 13 2D and 3D docking conformation of (a) **CHTUD2** and (b) **CHTUD3** inside the active site of LpxC (PDB: 4IS9).

donors. Similarly, the residue Ser116 formed two hydrogen bond donors with the oxygen of the pyranose ring and the hydroxyl group at C6 of the *N*-acetyl glucosamine ring (Glu-Nac), with bond lengths of 3.4 and 3.2 Å, resulting in bond strengths of 93 and 76%, indicating a favorable binding mode and a stable complex. Meanwhile, the glucosamine ring (Glu-N) established two hydrogen bond acceptors with the hydroxyl group at C3 and the oxygen of the pyranose ring, with bond lengths of 2.0 and 2.5 Å, and a bond strength of 30%, respectively. Additionally, hydrophobic interactions involving the trifluoromethyl, acetyl, and all hydroxyl groups within the **CHTUD3** backbone were observed (Fig. 11b).

To clarify and highlight the key functional groups in the synthesized **CHTUD1–3** that interact with the binding pocket of LpxC (PDB: 4IS9), a visualization analysis was conducted to explore the relationship between these interactions and the measured binding affinities. The binding affinities of the modified thiourea chitosan derivatives **CHTUD1–3** ranged from −12.72 to −14.58 kcal mol$^{-1}$. The interaction between the 4-fluorophenylthiourea chitosan derivative **CHTUD1** and the LpxC pocket exhibited a stable complex with a binding affinity of −12.72 kcal mol$^{-1}$. This interaction involved two hydrogen bond sidechain acceptors and three hydrogen bond donors, primarily interacting through the glucosamine ring (Glu-N). Meanwhile, the *N*-acetylglucosamine ring (Glu-Nac) displayed hydrophobic interactions with key amino acids in the pocket's active site through the fluoro atom of the aryl-thiourea derivative, the hydroxyl group attached to the pyranose ring, and the sulfur atom of thiourea of the molecule. The hydroxyl group at C3 of Glu-N formed hydrogen bonds with residues Lys239 and His265, with bond lengths of 2.3 and 3.1 Å, respectively. The hydroxyl group at C4 established a hydrogen bond as a sidechain donor with Thr191, with a bond length of 2.3 Å and a strength of 14%. Conversely, the hydroxyl group at C6 interacted with two key amino acids, Thr191 and Phe192, with bond lengths of 3.4 and 3.2 Å and strengths of 58 and 65%, respectively (Fig. 12).

In assessing the docking binding affinity of the 2,4-difluorophenylthiourea chitosan derivative, designated as **CHTUD2**, a value of −13.50 kcal mol$^{-1}$ was recorded. This affinity was primarily attributed to the formation of two hydrogen bonds involving sidechain acceptors between Thr191 and Lys239. These interactions were facilitated by the oxygen atom of the carbonyl group in the acetyl moiety of the Glu-Nac ring and the hydroxyl group at the C3 position of Glu-Nac, exhibiting bond lengths of 2.3 Å and 1.9 Å, with corresponding binding strengths of 37 and 65%, respectively. Furthermore, the hydroxyl group at C3 of Glu-Nac also acted as a backbone donor, establishing a hydrogen bond with the residue Met61, characterized by a bond length of 3.0 Å and a binding strength of 44% (Fig. 13a). Notably, docking studies of thiourea chitosan derivatives **CHTUD3** revealed significant flexibility in the binding pocket, with a binding affinity of −14.58 kcal mol$^{-1}$. These results demonstrated two hydrogen bonds formed by sidechain

donors between Thr191 and Glu78, involving hydroxyl groups at C3 and C6 of Glu-N, with bond lengths of 2.7 Å and 2.1 Å. Additionally, the NH of the acetyl group formed a hydrogen bond donor with the backbone of Met61, exhibiting a bond length of 1.8 Å and a strength of 27%. Furthermore, the phenyl group of the arylthiourea moiety establishes arene–cation interactions with Lys239, while **CHTUD3** displayed hydrophobic interactions with the amino acid residues in the active site (Fig. 13b).

Finally, the docking results indicated that thiourea-chitosan derivatives **CHTUD1–3** exhibited strong binding affinities inside the active sites of sortase A (PDB: 1T2P) and LpxC (PDB: 4IS9), suggesting that these derivatives may disrupt adhesion levels and membrane formation in *S. aureus* and *S. typhi* by forming stable and favorable interactions. These results may be aligned with biofilm-inhibitory and biocidal activities, which align with experimental data on antimicrobials and antibiofilms.

# 4. Conclusion

This research presents the successful preparation of three novel fluorinated chitosan derivatives based on a newly synthesized chitosan isothiocyanate derivative, which is grafted with promising fluorinated amines. Consistent with studies of ion-exchange capacity, quantitative $^1$H NMR examination verified a high substitution degree of 0.47 with the **CHTUD1** sample. Compared to the native chitosan, the chitosan thiourea derivative samples (**CHTUD1–3**) exhibited significantly reduced crystallinity and markedly enhanced thermal stability. Unmodified chitosan exhibited a crystallinity index of 72.12%, which systematically decreased upon modification to 53.44%, 53.13%, and 50.88% for derivatives **CHTUD1–3**, respectively. In addition, the chitosan-thiourea functionalization revealed superior thermal stability, with $T_{50}$ values of 341 °C (**CHTUD1**), 322 °C (**CHTUD2**), and 336 °C (**CHTUD3**), compared to pure chitosan (250 °C). The modified chitosan sample displayed enhanced solubility in DMF and DMSO compared with chitosan. Improving the material's antimicrobial capabilities was the most important result of this chemical modification. So, the three fluorinated chitosan thiourea derivatives were evaluated for their antimicrobial activities against two Gram-positive bacteria, two Gram-negative bacteria, and *C. albicans* as a fungal strain. All modified samples demonstrated greater potency than chitosan itself and showed promising activity compared to ampicillin and nystatin as a benchmark for the observed *in vitro* antimicrobial activity through *in vitro* studies. All modified samples exhibited a significant increase in antimicrobial potency compared to native chitosan, particularly compounds **CHTUD2** and **CHTUD3**, which showed potent activity against both Gram-positive and Gram-negative strains. The synthesized chitosan thiourea derivatives **CHTUD1–3** also displayed notable antifungal activity, with an MIC value of 15.62 μg mL$^{-1}$, compared to chitosan (MIC = 62.5 μg mL$^{-1}$). The structure–activity relationship (SAR) suggests that the incorporation of fluorinated groups can improve antimicrobial activity, mainly when these groups are situated at the *ortho* and *para* positions on the aromatic ring. Moreover, these derivatives demonstrated significantly improved bactericidal and fungicidal activities compared to native chitosan. The MBC and MFC values ranged from 15.62–62.5 μg mL$^{-1}$ and 15.62–31.25 μg mL$^{-1}$, respectively. The MIC values obtained indicate that the modified chitosan derivatives exhibit significant *in vitro* antimicrobial activity, comparable to that of the reference drugs under the tested conditions. However, any direct comparison should be interpreted with caution due to the inherent physicochemical and pharmacokinetic differences between the polymeric systems and conventional small-molecule antibiotics. Fluorinated thiourea-chitosan derivatives **CHTUD1–3** exhibited superior anti-biofilm properties against *S. aureus* and *S. typhi* compared to native chitosan. Enhanced biofilm integrity may result from the increased hydrophobicity and electrostatic interactions associated with the fluorine substitution, which facilitate adhesion to bacterial surfaces. *In silico* toxicity prediction was assessed and found to be generally non-toxic, showing no signs of cytotoxicity, mutagenicity, or carcinogenicity, except that **CHTUD2** and **CHTUD3** exhibited mild immunotoxic properties.

### 4.1. Future perspectives

Further research is necessary, as the fluorinated thiourea-chitosan sample (**CHTUD3**) exhibited an extremely high level of biological activity. Subsequent investigations must prioritize the optimization and scaling of the synthesis process to guarantee reproducibility and cost-effectiveness. To further assess the long-term biocompatibility, toxicity, and therapeutic effectiveness of these compounds, additional *in vivo* investigations are necessary. The adoption of this research int clinical applications, specifically for the creation of antimicrobial coatings for medical devices, advanced wound dressings, or drug delivery systems aimed at addressing multidrug-resistant pathogens, signifies a promising direction in the domain of functionalized carbohydrate polymers.

# Conflicts of interest

The authors declare that they have no conflicts of interest.

# Data availability

Supplementary information (SI) is available. See DOI: https://doi.org/10.1039/d6ma00145a.

# Acknowledgements

The authors extend their appreciation to the Deanship of Research and Graduate Studies at King Khalid University for funding this work through the Large Research Project under grant number RGP2/41/46.

## References

1 P. Dasí-Delgado, C. Andreu and M. del Olmo, *Molecules*, 2025, **30**, 2868.
2 R. D. Süssmuth, M. Kulike-Koczula, P. Gao and S. Kosol, *Angew. Chem., Int. Ed.*, 2025, **64**, e202414325.
3 R. H. Abd El-Aleam, R. F. George, H. H. Georgey and H. M. Abdel-Rahman, *RSC Adv.*, 2021, **11**, 36459–36482.
4 T. Qadir, A. Amin, P. K. Sharma, I. Jeelani and H. Abe, *Open Med. Chem. J.*, 2022, 2202280.
5 G. Satchanska, S. Davidova and P. D. Petrov, *Polymers*, 2024, **16**, 1159.
6 N. S. K. Gowthaman, H. N. Lim, T. R. Sreeraj, A. Amalraj and S. Gopi, *Biopolymers and their Industrial Applications*, Elsevier, 2021, pp. 351–372.
7 E. M. Elnaggar, M. S. Abusaif, Y. M. Abdel-Baky, A. Ragab, A. M. Omer, I. Ibrahim and Y. A. Ammar, *Int. J. Biol. Macromol.*, 2024, **277**, 134347.
8 M. M. Omran, M. M. Kamal, Y. A. Ammar, M. S. Abusaif, M. M. F. Ismail and H. H. Mansour, *Sci. Rep.*, 2024, **14**, 19818.
9 R. S. Alfinaikh, K. A. Alamry and M. A. Hussein, *RSC Adv.*, 2025, **15**, 4708–4767.
10 M. Gao, H. Tang and H. Zhu, *Compr. Rev. Food Sci. Food Saf.*, 2024, 70008.
11 R. K. Pavithran, S. G. Reddy, B. Siva Kumar and S. Kugabalasooriar, *ES Food Agrofor.*, 2025, 1–10.
12 S. Sigonya, B. M. Mothudi, O. J. Fakayode, T. C. Mokhena, P. Mayer, T. H. Mokhothu, T. R. Makhanya and K. Shingange, *Polymers*, 2025, **17**, 2082.
13 D. Zhuang, R. Li, S. Wang, H. N. Ahmad and J. Zhu, *Int. J. Biol. Macromol.*, 2024, **255**, 128043.
14 R. Wang, S. Xu, M. Zhang, W. Feng, C. Wang, X. Qiu, J. Li and W. Zhao, *Carbohydr. Polym.*, 2024, **342**, 122325.
15 V. Pawariya, S. De and J. Dutta, *Int. J. Biol. Macromol.*, 2024, **264**, 130664.
16 S. S. Alharthi, T. Gomathi, J. J. Joseph, J. Rakshavi, J. A. K. Florence, P. N. Sudha, G. Rajakumar and M. Thiruvengadam, *J. King Saud Univ., Sci.*, 2022, **34**, 102177.
17 A. A. Ali, H. Abd El-Wahab, M. S. Abusaif, A. Ragab, O. A. Abdel-Jaid, E. A. Eldeeb and Y. A. Ammar, *Pigm. Resin Technol.*, 2024, **53**, 557–568.
18 M. R. Rodrigues, *J. Carbohydr. Chem.*, 2005, **24**, 41–54.
19 M. Shibano, S. Nishida, Y. Saito, H. Kamitakahara and T. Takano, *Carbohydr. Polym.*, 2014, **113**, 279–285.
20 A. Bermúdez-Oria, G. Rodríguez-Gutiérrez, B. Vioque, F. Rubio-Senent and J. Fernández-Bolaños, *Carbohydr. Polym.*, 2017, **178**, 368–377.
21 D. Martínez-Cisterna, L. Chen, L. Bardehle, E. Hermosilla, G. Tortella, M. Chacón-Fuentes and O. Rubilar, *Int. J. Mol. Sci.*, 2025, **26**, 4130.
22 A. M. Fekry and R. R. Mohamed, *Electrochim. Acta*, 2010, **55**, 1933–1939.
23 Z. Zhong, R. Xing, S. Liu, L. Wang, S. Cai and P. Li, *Carbohydr. Res.*, 2008, **343**, 566–570.
24 M. Monier and D. A. Abdel-Latif, *J. Hazard. Mater.*, 2012, **209–210**, 240–249.
25 S. Bondock, A. A. El-Zahhar, M. M. Alghamdi and S. M. A. S. Keshk, *Int. J. Biol. Macromol.*, 2019, **137**, 107–118.
26 J. Fernández-Bolaños, B. Felizón, A. Heredia, R. Guillén and A. Jiménez, *Bioresour. Technol.*, 1999, **68**, 121–132.
27 M. Shibano, H. Kamitakahara and T. Takano, *Carbohydr. Res.*, 2013, **382**, 25–29.
28 F. Lafzi, D. Kilic, M. Yildiz and N. Saracoglu, *J. Mol. Struct.*, 2021, **1241**, 130566.
29 A. Khan, P. Dawar and S. De, *Bioorg. Chem.*, 2025, **158**, 108319.
30 A. R. Jennings and D. Y. Son, *Tetrahedron*, 2015, **71**, 3990–3999.
31 M.-O. M. Piepenbrock, G. O. Lloyd, N. Clarke and J. W. Steed, *Chem. Commun.*, 2008, 2644.
32 T. Venkatachalam, C. Mao and F. Uckun, *Bioorg. Med. Chem.*, 2004, **12**, 4275–4284.
33 J. Lee, S.-U. Kang, H.-K. Choi, J. Lee, J.-O. Lim, M.-J. Kil, M.-K. Jin, K.-P. Kim, J.-H. Sung, S.-J. Chung, H.-J. Ha, Y.-H. Kim, L. V. Pearce, R. Tran, D. J. Lundberg, Y. Wang, A. Toth and P. M. Blumberg, *Bioorg. Med. Chem. Lett.*, 2004, **14**, 2291–2297.
34 S. A. Khan, N. Singh and K. Saleem, *Eur. J. Med. Chem.*, 2008, **43**, 2272–2277.
35 A. P. Keche, G. D. Hatnapure, R. H. Tale, A. H. Rodge, S. S. Birajdar and V. M. Kamble, *Bioorg. Med. Chem. Lett.*, 2012, **22**, 3445–3448.
36 S. Saeed, N. Rashid, P. G. Jones, M. Ali and R. Hussain, *Eur. J. Med. Chem.*, 2010, **45**, 1323–1331.
37 R. Pingaew, N. Sinthupoom, P. Mandi, V. Prachayasittikul, R. Cherdtrakulkiat, S. Prachayasittikul, S. Ruchirawat and V. Prachayasittikul, *Med. Chem. Res.*, 2017, **26**, 3136–3148.
38 K. M. Khan, S. Saeed, M. Ali, M. Gohar, J. Zahid, A. Khan, S. Perveen and M. I. Choudhary, *Bioorg. Med. Chem.*, 2009, **17**, 2447–2451.
39 A. Ragab, M. A. Salem, Y. A. Ammar, W. M. Aboulthana, M. H. Helal and M. S. Abusaif, *Drug Dev. Res.*, 2024, **85**, e22216.
40 B. E. Smart, *J. Fluorine Chem.*, 2001, **109**, 3–11.
41 H. G. Bonacorso, A. P. Wentz, R. V. Lourega, C. A. Cechinel, T. S. Moraes, H. S. Coelho, N. Zanatta, M. A. P. Martins, M. Höerner and S. H. Alves, *J. Fluorine Chem.*, 2006, **127**, 1066–1072.
42 M. Jagodzinska, F. Huguenot, G. Candiani and M. Zanda, *ChemMedChem*, 2009, **4**, 49–51.
43 M. A. Salem, M. S. Abusaif, N. A. Gohar, Y. A. Ammar and A. Ragab, *Drug Dev. Res.*, 2025, **86**, e70085.
44 S. Shrimandilkar, P. Tryambake, S. Borgave and D. Lokhande, *J. Mol. Struct.*, 2025, **1345**, 141670.
45 E. A. Ali, H. M. Abo-Salem, A. A. Arafa and A. A. Nada, *Cellulose*, 2023, **30**, 3505–3522.
46 L. Yang, Y. Du, H. Wang and Y. Yang, *J. Cleaner Prod.*, 2025, **522**, 146351.
47 I. R. Fatika and F. Aligarh, in *International Conference on Islamic Economics (ICIE)*, 2024, vol. 1, pp. 324–332.
48 Z. Fu, W. Yuan, N. Chen, Z. Yang and J. Xu, *Green Chem.*, 2018, **20**, 4484–4491.

49 O. A. A. Ali, A. Ragab, Y. A. Ammar and M. S. Abusaif, *J. Mol. Struct.*, 2025, **1334**, 141879.
50 A. Zieba, D. Pindjakova, M. Latocha, J. Plonka-Czerw, D. Kusmierz, A. Cizek and J. Jampilek, *Molecules*, 2024, **29**, 4044.
51 A. Ragab, M. S. Abusaif, H. M. R. M. Selim, O. K. M. Riad, M. H. Helal, A. M. Ali, Y. A. Ammar and G. E. Ahmed, *Bioorg. Chem.*, 2025, **165**, 108977.
52 H. Khamees Thabet, A. Ragab, M. Imran, M. H. Helal, S. Ibrahim Alaqel, A. Alshehri, A. Ash Mohd, M. Rakan Alshammari, M. S. Abusaif and Y. A. Ammar, *Eur. J. Med. Chem.*, 2024, **275**, 116589.
53 H. F. Rizk, M. A. El-Borai, A. Ragab, S. A. Ibrahim and M. E. Sadek, *Polycyclic Aromat. Compd.*, 2023, **43**, 500–522.
54 M. A. Ismail, M. S. Abusaif, M. S. A. El-Gaby, Y. A. Ammar and A. Ragab, *RSC Adv.*, 2023, **13**, 12589–12608.
55 Y. M. Abdel-Baky, A. M. Omer, E. M. El-Fakharany, Y. A. Ammar, M. S. Abusaif and A. Ragab, *Sci. Rep.*, 2023, **13**, 22792.
56 D. D. Babu, A. S. Pani, S. D. Joshi, P. Naik, G. K. Jayaprakash, M. Al-Ghorbani, B. Rodrigues and B. K. Momidi, *Microb. Pathog.*, 2025, **200**, 107209.
57 H. Zaman, A. Saeed, H. Ismail and M. Rashid, *Arch. Biochem. Biophys.*, 2025, **765**, 110304.
58 Z. Fu, W. Yuan, N. Chen, Z. Yang and J. Xu, *Green Chem.*, 2018, **20**, 4484–4491.
59 K. Srivastava, A. Bhatt, N. Singh, R. Khare, R. Shukla, D. Chaturvedi and R. Kant, *Chem. Biol.*, 2020, **10**, 34–50.
60 M. M. Ghorab, M. S. A. El-Gaby, M. S. Alsaid, Y. A. M. M. Elshaier, A. M. Soliman, F. F. El-Senduny, F. A. Badria and A. Y. A. Sherif, *Adv. Anticancer Agents Med. Chem.*, 2017, **17**, 1411–1425.
61 R. Antony, S. Theodore David, K. Saravanan, K. Karuppasamy and S. Balakumar, *Spectrochim. Acta, Part A*, 2013, **103**, 423–430.
62 G. I. Edo, W. Ndudi, A. B. M. Ali, E. Yousif, K. Zainulabdeen, P. O. Akpoghelie, E. F. Isoje, U. A. Igbuku, R. A. Opiti, A. E. Athan Essaghah, D. S. Ahmed, H. Umar and A. A. Alamiery, *Carbohydr. Res.*, 2025, **550**, 109409.
63 Y. M. Abdel-Baky, A. Ragab, M. S. Abusaif, Y. A. Ammar and A. M. Omer, *Carbohydr. Polym.*, 2025, 124049.
64 Y. Peng, Y. Yu, Z. Su, Y. Zhong, S. Vijayakumar, Y. Chen, Y. Mao, M. Xin and M. Li, *Carbohydr. Polym.*, 2025, **367**, 124015.
65 M. M. Ahmed, N. T. I. Salama, S. Bondock, A. A. Soayed and R. M. I. Elsamra, *Appl. Organomet. Chem.*, 2025, 70125.
66 S. M. Tawfik, H. Jang, H. Kwon, M. Fekry, A. A. Roshdy, A. Ragab, B. Zakaria, M. Fouad, Y. A. Ammar and M. S. Abusaif, *Int. J. Biol. Macromol.*, 2023, 150699.
67 A. H. dos Reis-Prado, M. Rahimnejad, R. Dal-Fabbro, P. T. A. de Toledo, C. Anselmi, P. H. C. de Oliveira, J. C. Fenno, L. T. A. Cintra, F. Benetti and M. C. Bottino, *Bioact. Mater.*, 2025, **46**, 406–422.
68 R. K. Cheedarala, A. M. Kurumbala and R. R. Chidambaram, *Chem. Eng. J.*, 2025, **522**, 168263.
69 T. Alizadeh and Z. Asadi, *Carbohydr. Polym. Technol. Appl.*, 2025, **11**, 100997.
70 R. Malav, R. K. Sharma and S. Ray, *Int. J. Biol. Macromol.*, 2025, **301**, 140338.
71 Y. M. Abdel-Baky, A. Ragab, M. S. Abusaif, Y. A. Ammar and A. M. Omer, *Carbohydr. Polym.*, 2025, **368**, 124049.
72 N. D. Alharbi, H. H. Amer, N. A. El-Zaher and O. W. Guirguis, *Polym. Polym. Compos.*, 2022, **26**, DOI: 10.1177/09673911221148826.
73 F. J. Caro-León, E. Silva-Campa, R. A. Navarro-López, D. Fernández-Quiroz, V. A. Figueroa-León, M. A. Trujillo-Ramirez, L. M. López-Martínez, M. R. Aguilar and O. Álvarez-Bajo, *ACS Omega*, 2025, **10**, 3474–3485.
74 A. Ragab, D. M. Elsisi, E. M. Elqady, E. EL-Said, M. A. Salem, Y. A. Ammar and M. S. Abusaif, *Pestic. Biochem. Physiol.*, 2024, **202**, 105943.
75 H. R. Mardani, F. Ravari, A. Kalaki and L. Hokmabadi, *J. Polym. Environ.*, 2020, **28**, 2523–2538.
76 P. Khosravian, R. Mardani, Z. K. Boldaji, M. Javdani and M. Hashemnia, *Naunyn-Schmiedeberg's Arch. Pharmacol.*, 2025, 1–19.
77 A. Ragab, R. Ayman, M. A. Salem, Y. A. Ammar and M. S. Abusaif, *Eur. J. Med. Chem.*, 2025, **290**, 117499.
78 M. S. A. El-Gaby, Y. A. Ammar, M. A. Ismail, A. Ragab and M. S. Abusaif, *Heterocycl. Commun.*, 2023, DOI: 10.1515/hc-2022-0170.
79 X. Han, W. Lv, S.-Y. Guo, M. Cushman and J.-H. Liang, *Bioorg. Med. Chem.*, 2015, **23**, 6437–6453.
80 M. S. A. El-Gaby, Y. A. Ammar, M. A. Ismail, A. Ragab and M. S. Abusaif, *Heterocycl. Commun.*, 2023, **25**, DOI: 10.1515/hc-2022-0170.
81 Y. A. Ammar, J. A. Micky, D. S. Aboul-Magd, S. M. A. Abd El-Hafez, S. A. Hessein, A. M. Ali and A. Ragab, *Chem. Biol. Drug Des.*, 2023, **101**, 245–270.
82 R. R. Raslan, Y. A. Ammar, S. A. Fouad, S. A. Hessein, N. A. M. Shmiess and A. Ragab, *RSC Adv.*, 2023, **13**, 10440–10458.
83 M. M. F. Ismail, T. Z. Shawer, R. S. Ibrahim, M. S. Abusaif, M. M. Kamal, R. M. Allam and Y. A. Ammar, *RSC Adv.*, 2023, **13**, 31908–31924.
84 H. K. Thabet, A. Ragab, M. Imran, M. Hamdy Helal, S. Ibrahim Alaqel, A. Alshehri, A. Ash Mohd, S. S. Alshammari, Y. A. Ammar and M. S. Abusaif, *RSC Adv.*, 2024, **14**, 15691–15705.
85 H. Khamees Thabet, Y. A. Ammar, M. Imran, M. Hamdy Helal, S. Ibrahim Alaqel, A. Alshehri, A. Ash Mohd, M. S. Abusaif and A. Ragab, *Bioorg. Chem.*, 2024, **151**, 107671.
86 A. Ragab, M. S. Abusaif, N. A. Gohar, D. S. Aboul-Magd, E. A. Fayed and Y. A. Ammar, *Bioorg. Chem.*, 2023, **131**, 106307.
87 G. A. Abd-elmaksoud, M. S. Abusaif, Y. A. Ammar, S. Al-Sharbasy and M. A. Migahed, *Arabian J. Sci. Eng.*, 2023, **48**, 16167–16185.
88 A.-M. Möller, M. Vázquez-Hernández, B. Kutscher, R. Brysch, S. Brückner, E. C. Marino, J. Kleetz, C. H. R. Senges, S. Schäkermann, J. E. Bandow and F. Narberhaus, *J. Biol. Chem.*, 2024, **300**, 107143.
89 M. S. Abusaif, A. Ragab, E. A. Fayed, Y. A. Ammar, A. M. H. Gowifel, S. O. Hassanin, G. E. Ahmed and N. A. Gohar, *Bioorg. Chem.*, 2025, **154**, 108023.